DNA 4182F

A SIMPLIFIED MODEL OF SHOCK-ON-SHOCK INTERACTION

Martin Marietta Aerospace
Sand Lake Road
Orlando, Florida 32805

September 1976

Final Report for Period February 1976 — September 1976
CONTRACT No. DNA001-76-C-0175

Approved for public release; distribution unlimited.

Prepared for

Headquarters
DEFENSE NUCLEAR AGENCY (SPAS)
Washington, D.C. 20305

D D C

MAR 29 1977

C

REPORT DOCUMENTATION PAGE		READ INSTRUCTIONS BEFORE COMPLETING FORM
1. REPORT NUMBER 19 DNA 4190F	2. GOVT ACCESSION NO.	3. RECIPIENT'S CATALOG NUMBER
4. TITLE (and Subtitle) A Simplified Model of Shock-on-Shock Interaction		5. TYPE OF REPORT & PERIOD COVERED Final Report (DRAFT) February 30 1976 — 30 Sep 76
		6. PERFORMING ORG. REPORT NUMBER OR-14,282
7. AUTHOR(s) G. F. Aiello		8. CONTRACT OR GRANT NUMBER(s) DNA 001-76-C-0175
9. PERFORMING ORGANIZATION NAME AND ADDRESS Martin Marietta Corporation Post Office Box 5837 Orlando, Florida 32805		10. PROGRAM ELEMENT, PROJECT, TASK AREA & WORK UNIT NUMBERS
11. CONTROLLING OFFICE NAME AND ADDRESS Director Defense Nuclear Agency Washington, D. C. 20305		12. REPORT DATE August 1976
		13. NUMBER OF PAGES 76
14. MONITORING AGENCY NAME & ADDRESS(if different from Controlling Office)		15. SECURITY CLASS. (of this report) Unclassified
		15a. DECLASSIFICATION/DOWNGRADING SCHEDULE

16. DISTRIBUTION STATEMENT (of this Report)

Approved for public release; distribution
unlimited.

17. DISTRIBUTION STATEMENT (of the abstract entered in Block 20, if different from Report)

403238

19. KEY WORDS (Continue on reverse side if necessary and identify by block number)

Blast	Experiment Test
Shock	Hypersonic
Sled Test	Cone
Pressure	

20. ABSTRACT (Continue on reverse side if necessary and identify by block number)

A simplified model is presented of the shock-on-shock problem as it pertains
to the encounter between a supersonic cone and a planar blast wave. The model
provides an accurate and inexpensive means of predicting the circumferential
distribution of peak pressures and pulse duration for all encounter angles
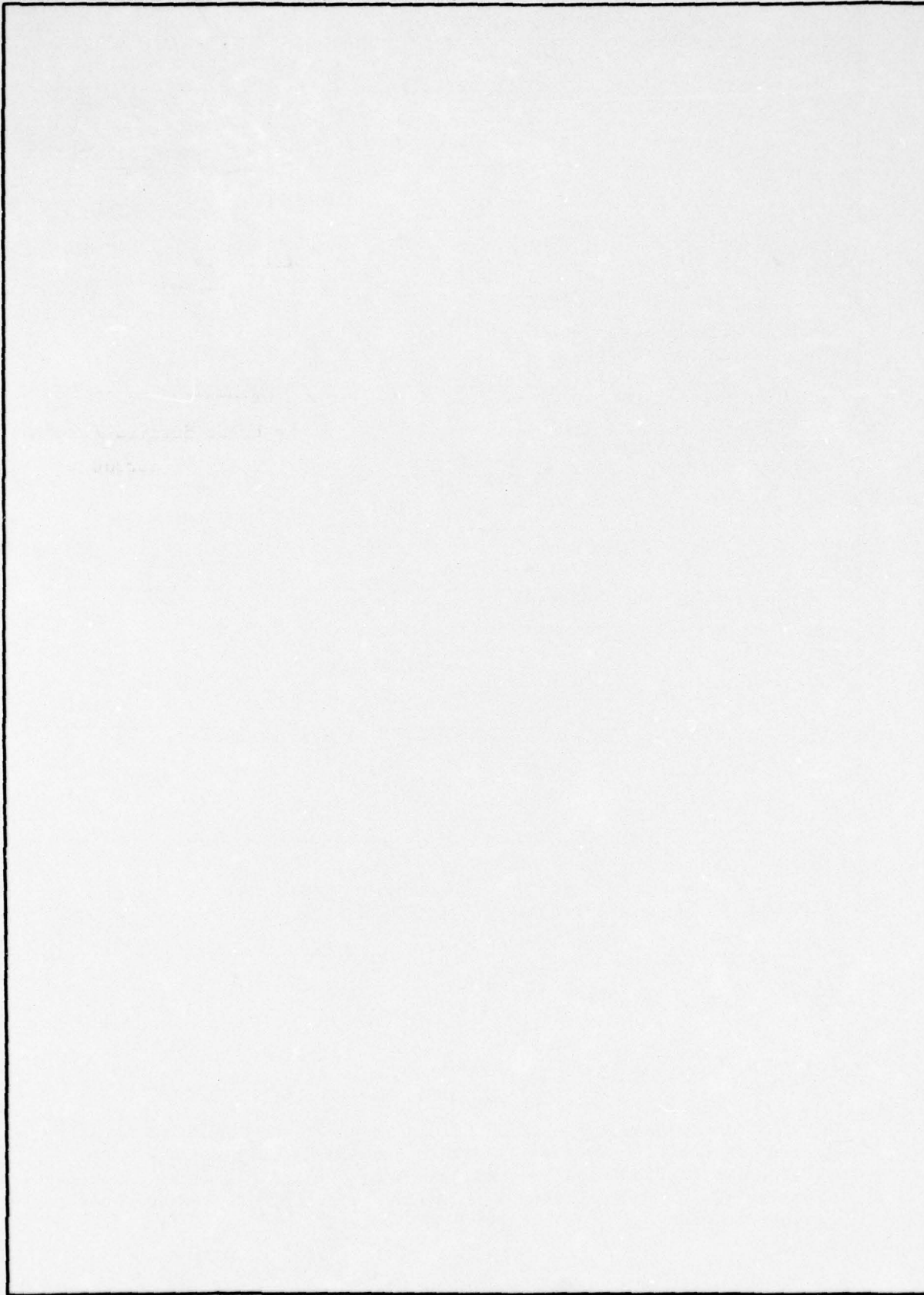between nose-on and broadside with the cone at zero or small angles of attack.

DD FORM 1473 1 JAN 73   EDITION OF 1 NOV 65 IS OBSOLETE

SUMMARY

The shock—on—shock phenomenon represents a potentially dangerous environment to high performance strategic interceptors. Therefore, there is a need to have the capability to predict the pressure distribution history due to such encounters. The objective of this program was to develop a computerized model which is inexpensive to operate as well as accurate. The knowledge required to simplify the model is derived from the Defense Nuclear Agency sled test data and the NASA Ames rigorous analytical results.

The model presented here permits prediction of the circumferential distribution of peak pressures that result from an encounter at any angle from nose—on to broadside. The sharp supersonic conical body may also be at a small (less than the cone half—angle) angle of attack. The model also allows prediction of the circumferential distribution of the duration of the shock—on—shock pulse which is defined as the time it takes for the surface pressure to reach the "quasi—steady" pressure level associated with complete engulfment of the vehicle. Finally, the model permits estimating the engulfment time of a particular axial station of the vehicle, i.e., the time interval between the arrival of the wave front at the subject station on the windward side of the cone and the arrival at that station on the leeward side.

Comparisons between the new model and the existing data show good agreement and, where no comparisons are possible, the new results are plausible. In spite of the simplifying assumptions and some empiricism, the model is expected to be effective over a fairly large range of blast and vehicle conditions except for angle of attack. When the angle of attack increases to the point of flow separation on the leeside of the cone, the model no longer applies; it could, however, be modified to do so.

PREFACE

This final report discusses the "Development of a Simplified
Model of Shock-on-Shock Interaction" effort conducted by Martin
Marietta Aerospace Orlando Division, under Contract DNA001-76-C-0175,
for the Defense Nuclear Agency, Washington, D.C. The reporting period
is from February 1976 to September 1976.

The author wishes to acknowledge the vigorous interest and
support of Capt. David Garrison who is the Contract Officer Repre-
sentative for the Defense Nuclear Agency.

In addition, an expression of gratitude is given to Dr. Paul Kutler
of NASA Ames and Dr. Leonidas Sakell of Martin Marietta for providing
the predictions made with the Ames three-dimensional shock-on-shock
interaction solution.

The author also wishes to acknowledge the effort of Mr. Dean Cole
of KAMAN Nuclear for providing the digitized sled test data used in
this study.

CONTENTS

ILLUSTRATIONS

1.0   INTRODUCTION

The shock-shock interaction phenomenon occurs when a supersonic
vehicle encounters a shock wave. Recent interest in this problem is
due to the high probability of such an occurrence during the defense
of the Minuteman system by an interceptor. The threat of many reentry
vehicles attacking a single target necessarily results in a fratricidal
environment being created for an interceptor by the detonations of pre-
ceding interceptors. Such an encounter results in high frequency shocks
transmitted through substructure which can damage components. The sur-
face pressure is usually maximum immediately behind the wave which
strikes the surface of the vehicle and then it decays to a "quasi-
steady" value. The latter pressure is referred to as quasi-steady
because the apparently steady conditions will actually vary as the
vehicle traverses the blast sphere. However, relative to the short
time it takes for the vehicle to be engulfed by the wave, the conditions
behind the blast front may be assumed to be steady and the surface
pressure similarly achieves a steady value. The time to decay to
quasi-steady pressure is defined as the pulse duration.

The objective of this effort was to produce a relatively simple,
but accurate model of the shock-on-shock phenomenon as it occurs when
a sharp supersonic conical vehicle encounters a planar blast wave.
The desire is to be able to predict the following features of the
phenomenon, namely, the peak pressures and pulse durations produced
along the windward and leeward rays of the cone and the circumferen-
tial distributions of these quantities. Any encounter angle from
nose-on to broadside is permitted and the cone may be at small (less
than the cone half-angle) angles of attack. The requirement for
simplicity stems from the need for a low cost computer model.

5

The approach taken in structuring the model was to formulate a set of simplified assumptions based on the knowledge gained from: 1) the rigorous analytical results of Reference 1, 2) the test results of Reference 2, and 3) Reference 3 which presents a comparative study between these sources and established the framework for the model presented herein.

The following description of the problem (Section 2.0) is excerpted from Reference 3. Section 3.0 summarizes the current model and presents comparisons with other data sources. A listing is presented in Section 4.0 along with user information pertaining to the computerized version of the program.

2.0   THE PROBLEM – A FUNCTION OF ENCOUNTER ANGLE

The encounter between a blast wave and a supersonic vehicle
produces a highly transient pressure pulse which varies in strength
and duration depending on a combination of parameters: geometry and
flight condition of the vehicle and the strength and orientation of the
blast wave relative to the surface of the vehicle. Interest here is
limited to sharp cones so the vehicle condition at a given altitude
is defined by a combination of cone angle (θ_c), angle of attack (α),
and vehicle velocity (V). The strength of the blast wave is defined
by the ratio of the pressure behind to the pressure in front of the
wave (P_2/P_1) as it travels through the atmosphere. The encounter
angle (β) is defined as the angle between the blast wave and the
perpendicular to the vehicle axis as shown in Figure 1.
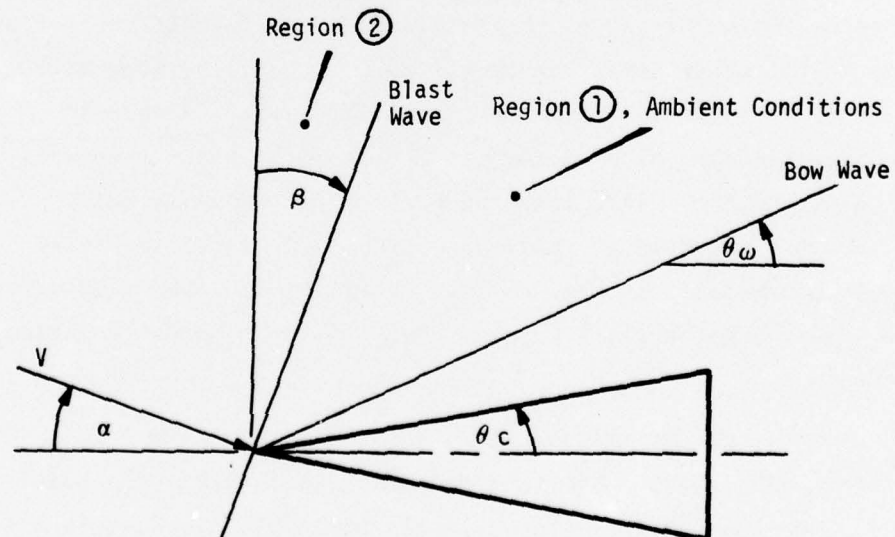
Figure 1.   Blast Wave – Vehicle Encounter Geometry

7

The primary determinant in the level of pressure is the strength of the blast wave, but the encounter angle (β) also plays an important role. As β varies from nose-on to broadside, several distinct classes of encounters can be identified. One subdivision of encounters is marked by the bow wave angle. For β's between nose-on ($\beta=0$) and parallel to the bow wave angle (i.e., $\beta=90 - \theta_w$), the intersection of the blast and bow waves during engulfment moves from the apex of the cone aftward. For β's between $(90 - \theta_w)$ and $(90 - \theta_c)$, the blast-bow wave intersection moves forward along the bow wave. The two cases must be, in general, treated separately.

The range of β's between nose-on and $(90 - \theta_w)$ must be subdivided further because the nature of the wave pattern which develops on the surface varies from Mach reflection to regular reflection as the encounter varies from nose-on towards broadside. The two types of wave pattern are illustrated in Figures 2a and 2b respectively. Unless a solution of the complete flow field is developed, as was done in Reference 1, the two types of wave patterns must be treated separately because there is, otherwise, no precise way of predicting the location and/or height of the Mach stem. The regular reflection pattern, on the other hand, can be solved rigorously as long as the transmitted and reflected waves are straight, i.e., immersed in uniform flow fields. As discussed in Section 3.1, the presence of gradients in the flow field leads to bending of the waves which complicates the solution of the wave pattern. It is shown that acceptable approximations are possible, however, and that good agreement is achieved between the simple model and the rigorous solution of Reference 1.

Encounters near broadside, where $(90 - \theta_w) \leq \beta \_ (90 - \theta_c)$, must also be subdivided into two subclasses depending on the orientation of the waves which emerge from the blast bow wave interaction. While the blast-bow wave intersection moves forward, the point of

8

intercept at the vehicle surface may move from front to back depending on the orientation of the wave transmitted to the surface as shown in Figure 3.

A. Mach Reflection   B. Regular Reflection
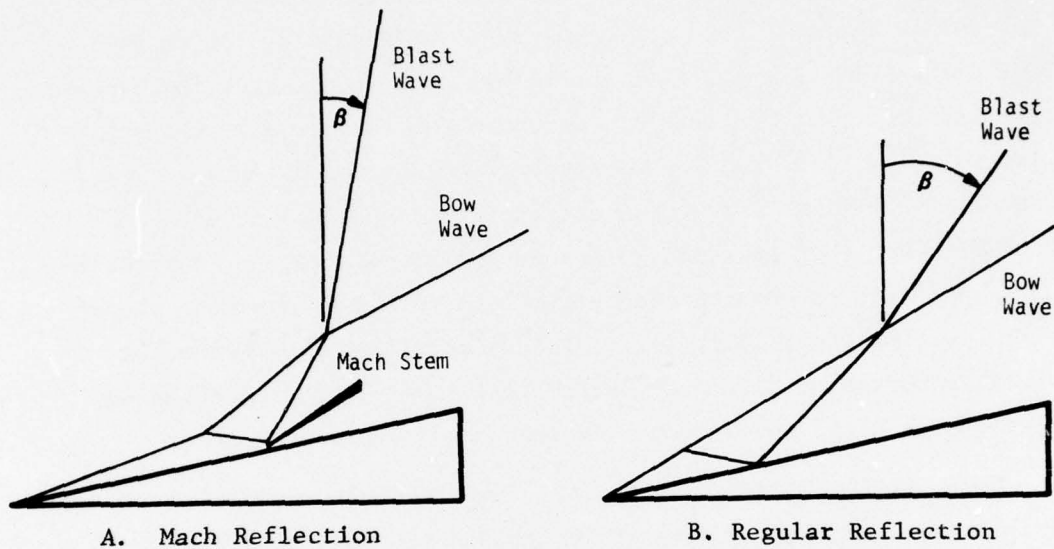
Figure 2. Wave Patterns with Varying Encounter Angle
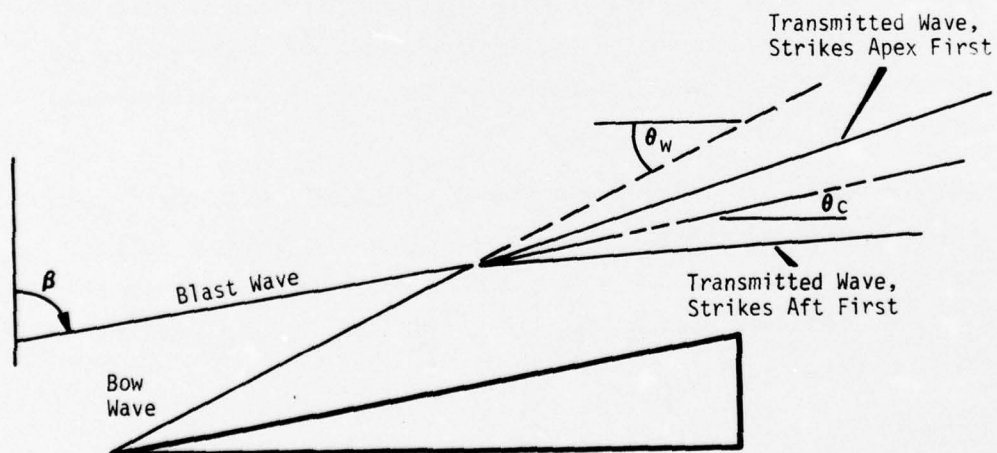
Figure 3. Two Possible Transmitted Wave Geometries

9

A regular reflection will occur in either case, but any attempt to model the phenomena must reflect the differences to correctly describe the velocity of the transmitted wave relative to the gas at the vehicle surface.

The complexities associated with the various subclasses of encounters are manifested in the development of models of the shock-shock phenomena. The earliest analytical success occurred for nose-on encounters which are further divided into two subclasses: sharp and blunt vehicles. The nose-on encounter of a slender sharp cone was treated by Inger in Reference 4 and the blunt body was treated successfully by McNamara and Taylor in References 5 and 6, respectively. It was possible to demonstrate the success of these solutions because of the test data available (e.g., References 7 and 8). Meanwhile, solutions were also developed for oblique encounters, but remained unverifiable until the recent sled test data became available.

Probably the highest quality experiments involving oblique encounters produced previously were the White Oak Laboratory of the Naval Surface Weapons Center using a ballistic range in combination with a shock tube. Excellent photographic data (References 9 and 10) were taken, but the use of ballistic models precluded the acquisition of actual pressure measurements. Thus, actual pressure measurements were limited essentially to nose-on encounters because of the limitations of the test techniques.

Interestingly, the sled tests cannot be used to simulate nose-on encounters because of interference between the wave and the ground. However, the sled test scheme does permit simulation of Mach stem, regular, and broadside encounters, thereby filling a large gap in the body of test data.

3.0 SHOCK-ON-SHOCK MODEL

The description of the model discussed in this section is sub-
divided in segments. The peak pressure on the windward ray of the cone
is analyzed, followed by the model of the peak pressure on the leeward
ray. The corresponding analyses of the windward and leeward pulse
durations are then presented, followed by a discussion of the circum-
ferential distributions.

The rationale presented here is used for both zero and non-zero
angle of attack (α) by replacing the real cone angle (θ_c) by an effec-
tive cone (Figure 4). The windward ray analysis was performed on an
effective cone with semi-vertex angle of $\theta_c + \alpha$ at zero angle of attack,
while in the leeward ray analysis, the semi-vertex angle is $\theta_c - \alpha$.
Similarly the bow wave angle is measured from the centerline of the
effective cone.
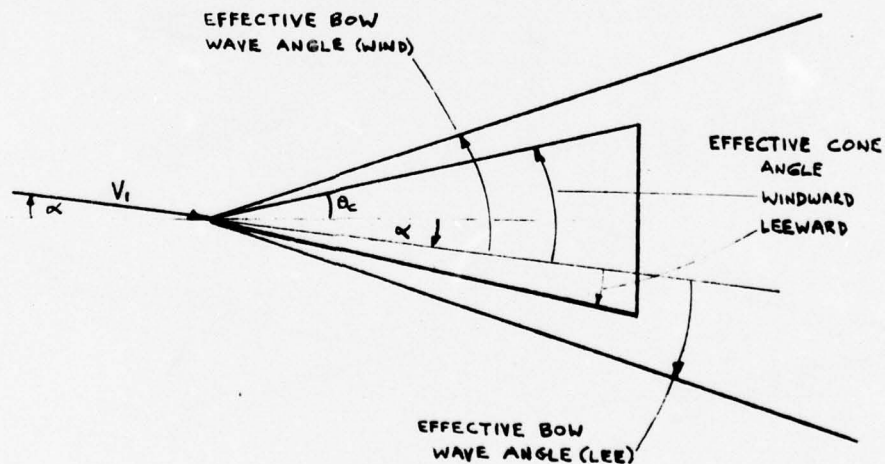
Figure 4. The Cone at Angle of Attack

11

3.1 Peak Windward Pressure

The starting point for the analysis was to examine some results
taken from Kutler and Sakell (Reference 1) and shown in Figure 5.
Figure 5 shows the isobar maps calculated with the Kutler solution
for an 11.2-degree half-angle cone at Mach 5. The isobars show the
shock wave patterns that result when the cone encounters a blast wave
of strength 1.6 (i.e., P_2/P_1) at six different encounter angles. At
the nose-on encounter ($\beta=0$), the wave transmitted to the surface is
very nearly straight. As the encounter angle becomes oblique, the
transmitted wave is seen to be curved. It was decided in formulating
the new model referred to here that the curvature in some form should
be considered.
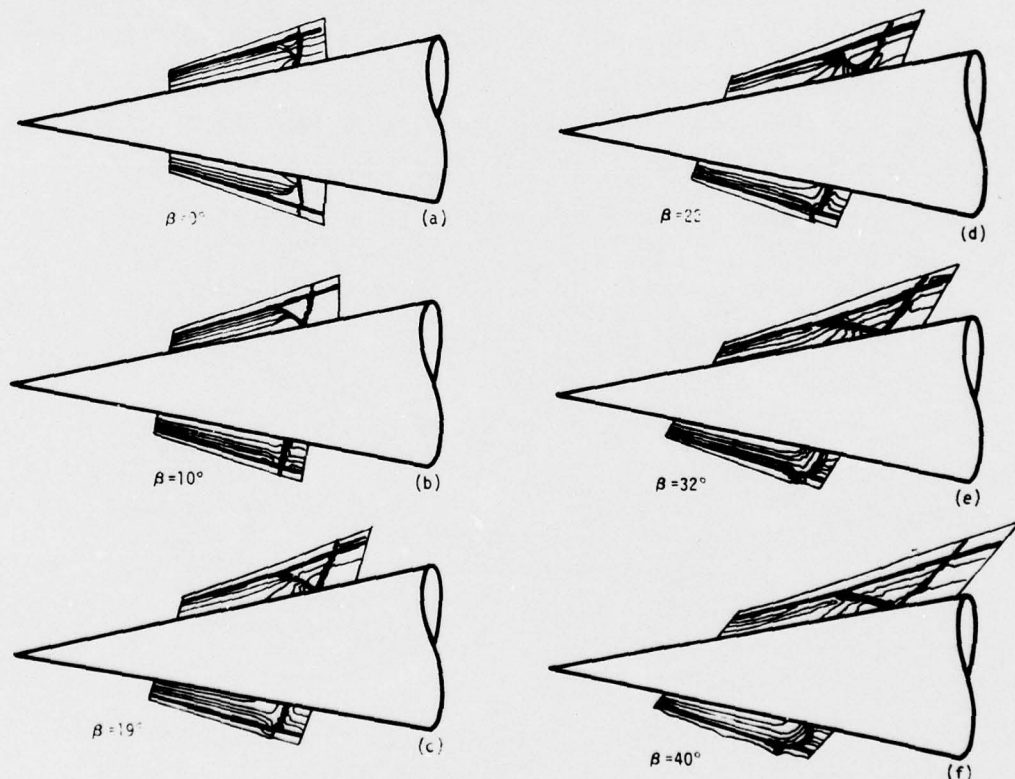
Figure 5. Windward and Leeward Isobar Maps at Selected Encounter Angles

12

Careful examination of the isobar maps shows that the height of the stem formed on the windward ray of the cone is relatively small in comparison to the shock layer thickness. The reflected wave bends away very quickly from being perpendicular to the surface to assume an orientation which is compatible with the new bow wave forming on the vehicle as a result of being immersed in the post-blast flow field. In fact, at all of the calculated cases except nose-on, the reflected wave bends almost immediately upon leaving the surface.

At some encounter angle between nose-on and 40 degrees, the wave pattern changes from Mach stem to regular reflection. Furthermore, as might be expected, there is no abrupt change in the wave pattern as the encounter angle changes from one which produces regular reflection to one which produces a Mach stem. Stated another way, it appears that the transmitted wave shape and orientation right down to the surface may be determined without regard for the type of reflection which will occur. If the transmitted wave is described properly, then the test for regular reflection is made at the surface and the peak pressure may be calculated accordingly, i.e., as the pressure behind a regular reflection or as the pressure behind a small normal shock located at the point of impingement of the transmitted wave on the surface.

The queston is how to solve for the bent transmitted wave in a simple fashion. The Kutler solution accomplishes this by subdividing the shock layer into many small segments and solves for the changes in flow conditions from point to point in the grid. The many points in the grid result in a more rigorous solution and increased computer cost. Noting that the transmitted wave actually is not highly curved, it was decided that the curved wave might be reasonably approximated with two straight segments as indicated in Figure 6. An iterative procedure is used to solve for the outer segment of the transmitted

13

wave by solving the two-shock interaction at the point where the bow and blast waves intersect.

Both waves are assumed to be locally two-dimensional and their interaction results in two waves which are the beginnings of the post-encounter bow wave and the transmitted wave, respectively. The rationale used in solving the interaction of two planar waves is:

1 Assume a value for pressure jump across wave P-R (Figure 6)

2 Calculate the flow direction in region 4 (Figure 6)

3 Calculate the flow direction in region 5, assuming the pressure in region 4

4 If the flow directions in regions 4 and 5 (Figure 6) agree then the solution is found, otherwise the procedure is repeated with a new pressure jump assumed in step one.
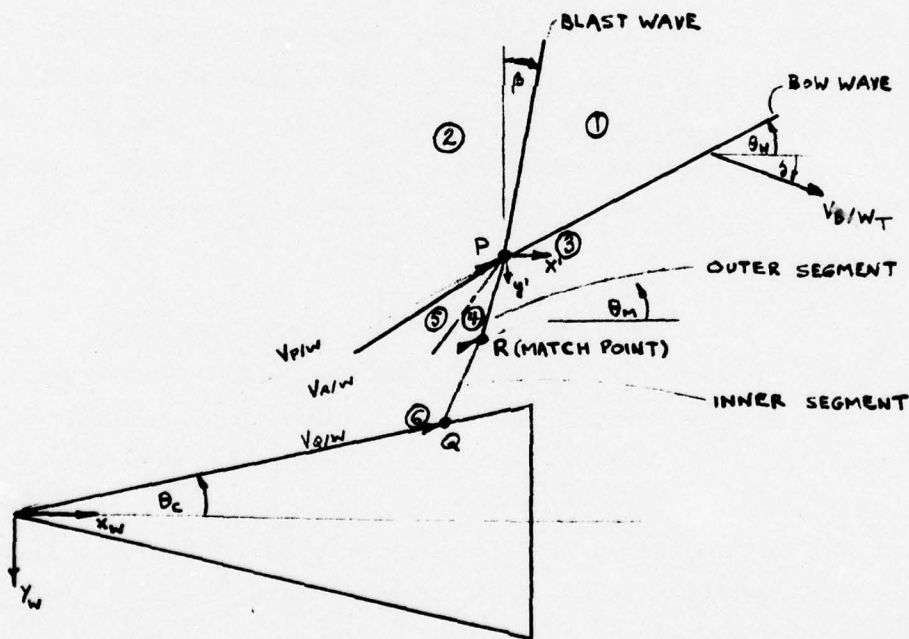
Figure 6. An Approximation to the Windward Transmitted Shock Wave

The key equations defining the above procedure are summarized below. To solve for the system of shock waves which result from the intersection of the blast and bow waves, it is useful to place the frame of reference at the point of intersection (P, Figure 6). The velocity of point P, along the bow wave, relative to the body fixed coordinates (x_W, y_W) is

$$V_{P/W} = V_{B/W_T} \frac{\cos (\beta-\delta)}{\cos (\beta+\theta_W)} \tag{1}$$

where V_{B/W_T} is the velocity of the blast relative to the body. In regions 1, 2, and 3 of Figure 6, the flow velocity components in the x' and y' directions relative to point P are

$$u_{1/P} = u_{1/W} - u_{P/W} \quad u_{2/P} = u_{2/W} - u_{P/W} \quad u_{3/P} = u_{3/W} - u_{P/W}$$

$$v_{1/P} = v_{1/W} - v_{P/W} \quad v_{2/P} = v_{2/W} - v_{P/W} \quad v_{3/P} = v_{3/W} - v_{P/W}$$

where

$$u_{P/W} = V_{P/W} \cos \theta_W$$

$$v_{P/W} = V_{P/W} \sin \theta_W$$

$u_{1/W}, v_{1/W}$ = Components of freestream velocity

$u_{2/W}, v_{2/W}$ = Components of post blast flow velocity

$u_{3/W}, v_{3/W}$ = Components of the shock layer velocity

relative to the body.

and $\delta = \tan^{-1} \left(\dfrac{u_{B/W}}{v_{B/W}} \right)$.

The velocity components define the flow direction in each region. By postulating a pressure jump across the outer segment of the transmitted wave, the oblique shock relations (e.g., see Reference 11) permit calculation of the flow direction in region 4. The same shock relations are used to calculate the flow direction in region 5, on

15

the condition that $P_5 = P_4$. This iterative procedure is continued until the flow directions in regions 4 and 5 are equal.

The outer segment of the transmitted wave, thus determined, is assumed to remain straight and of constant strength half-way into the shock layer. The match point (R, Figure 6) location and velocity $(V_{R/W})$ are determined by the point of intercept between the outer segment of the transmitted wave and the midpoint of the shock layer defined by

$$\theta_M = (\theta_W - \theta_c)/2 \tag{2}$$

and

$$V_{R/W} = V_{P/W} \frac{\sin (E_1 - \theta_W)}{\sin (E_1 - \theta_M)} \tag{3}$$

Knowing the pre-interaction conditions at the center of the shock layer, the pressure behind the transmitted wave outer segment is defined. The compatible inner segment is found by assigning values to the orientation of the inner segment and by calculating the resulting pressure jump at the surface. The wave strength calculated at the surface is presummed to apply along the entire inner segment and so the pressure behind the inner segment at the center of the shock layer may be calculated. The solution is found when the pressure calculated behind the inner segment at the match point agrees with the value calculated behind the outer segment. In this manner, the outer portion of the transmitted wave is consistent with the blast-bow interaction, the inner segment is consistent with the wave-surface interaction, and the two segments are compatible with each other to the extent that the pressure behind the two segments at the junction point is matched.

The calculation made at the surface begins with an attempt to find a regularly reflected wave which satisfies the condition that the flow must be parallel to the surface. If none is found, then a Mach

16

stem, which is infinitesimal in height, is presumed to exist. That
is, the stem is located at the point where the inner segment of the
transmitted wave impinges on the surface. This determines the
velocity of the impingement point relative to the surface $(V_{Q/W})$

$$V_{Q/W} = V_{R/W} \frac{\sin (E_2 - \theta_M)}{\sin (E_2 - \theta_c)} \quad . \tag{4}$$

The velocity of the point, Q, relative to the gas on the cone surface
is therefore also defined which, in turn, determines the strength of
the wave travelling along the surface.

The Rankine-Hugoniot equations are then used to calculate the
pressure jump across the normal shock. The key assumptions are that
the transmitted wave is not so curved that a two piece representation
is not adequate and that the Mach stem, when it occurs, is small in
extent relative to the height of the shock layer. In principle, the
matching of pressure only at the point of bending of the transmitted
wave is incomplete because the flow directions should also be matched.

It was not possible to retain the simplicity of the approach and
match flow directions too. Meanwhile, the comparisons with the Ames
peak windward pressures at a variety of conditions show agreement
to within about 10 percent. Furthermore, a considerable advantage is
gained in computation time because the new model requires just a few
seconds of CPU time on the IBM 370/158 at Martin Marietta's Orlando
Division.

With two exceptions, the new model treats the peak windward
pressure from nose-on to broadside since provision was made for the
possibility for the forward moving intercept point.

One exception occurs when the blast wave is exactly parallel to
the bow wave. Solving the interaction between the blast and bow

17

waves involves defining the local flow velocities relative to the intersection of the two waves. When the waves are parallel, the intersection point velocity approaches infinity, so a solution is not possible. Loss of the solution at the single value of encounter angle is not seen to be a serious matter. The second limitation occurs at the transition encounter angle, i.e., where the wave pattern changes from Mach stem to regular reflections, because the pressure function appears to be discontinuous. Even so, the error in pressure is on the order of 10 percent. As with the Ames model, the new model has not been exercised to the point where the limits of applicability are well defined; therefore, a complete judgment of this point cannot be made at this time.

The foregoing analysis was computerized and used to calculate the peak windward ray pressures at the set of conditions which were tested during the Holloman AFB sled test program described in Reference 2 (see Table 1). For a number of the conditions, predictions are also calculated with the method of Reference 1 and provided by Kutler in Reference 12.

Table 1. Sled Test Conditions, Phases II and III

Test Number	Cone Half-Angle(Deg)	Mach Number	Angle of Attack (Deg)	Blast Strength P2/P1	Encounter Angles (Deg)
B-2*	11.2 (Model 1)	5	0	1.8	22.2, 26.3 33, 78.4
B-3				2.2	24.9, 28.8, 33.2, 78.1
B-4				2.2	24.9, 31.8, 41.2, 78.2
B-5				2.6	22.2, 28.9, 36.9, 86.5
B-6					24.7, 31.8, 45.0, 64.0
B-7	6 (Model 2)				24.8, 36.9, 44.9, 62.8
B-8	11.2 (Model 1)	2.6			24.8, 36.7, 45.0, 66.3
B-9		5	5		17.9, 21.9, 31.3, 78
B-10		5	5		28, 32, 41

*Test B-1 was aborted.

Figure 7 shows the peak windward pressures plotted against encounter angle (β) including test data, Kutler's results, and the curves produced with the model discussed here.

A number of observations are possible regarding these comparisons. Good agreement is indicated between the simple model and the rigorous solution of Kutler. There is apparently poor agreement between the calculated values and the test data. However, as explained in References 2 and 3, the test data are expected to be lower than the predictions, particularly in the Mach stem regime because the pressure data acquisition system used in the sled tests did not have a rapid enough response time to record the peak. Reference 2 shows that when the response lag is considered, the Kutler results agree very well with the test data. Therefore, the Kutler solution is treated here as the standard for comparison.

3.2 Peak Leeward Pressure

Along the leeward ray of the cone, the transmitted wave pattern is a Mach stem regardless of encounter angle. Furthermore, the Kutler results show that as the encounter angle varies from nose-on to broad-side, the peak pressure does not always exceed the quasi-steady value. Thus, there is not necessarily a pressure overshoot. In this case, the pressure immediately behind the transmitted wave is less than the quasi-steady pressure and it rises monotonically to the quasi-steady value. Therefore, the approach taken in formulating the current leeward pressure model is to combine a method for calculating the pressure behind the transmitted wave with a method for calculating the quasi-steady pressure. Both quantities are calculated at each encounter angle and the applicable peak pressure is the higher of the two. Typically from $\beta=0$ (nose-on encounter) to some $\beta=\beta_{QS}$, the pressure behind the transmitted wave exceeds the quasi-steady pressure. For $\beta>\beta_{QS}$, the peak pressure is the quasi-steady value

19
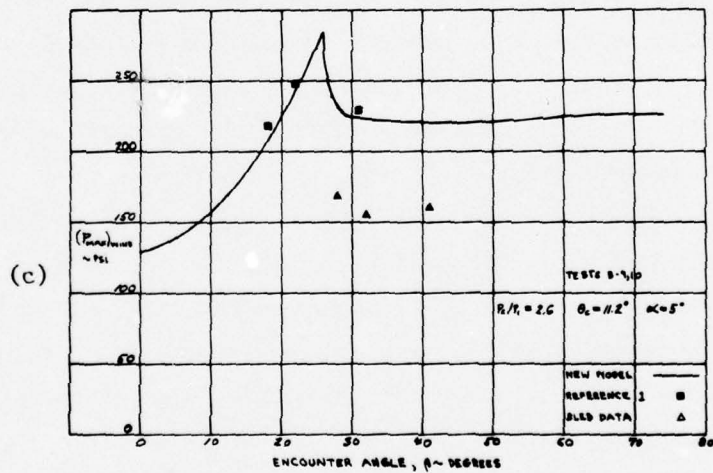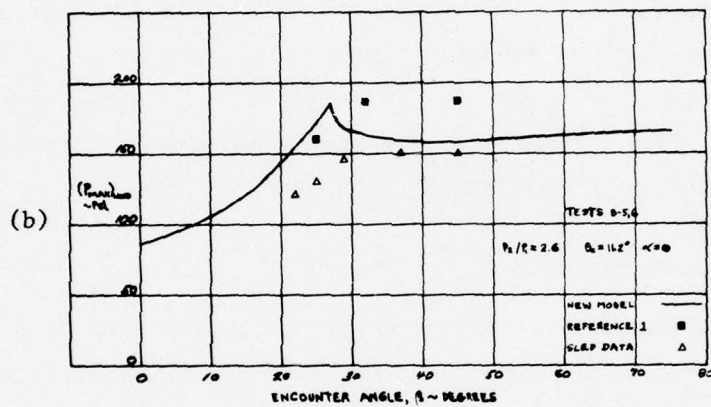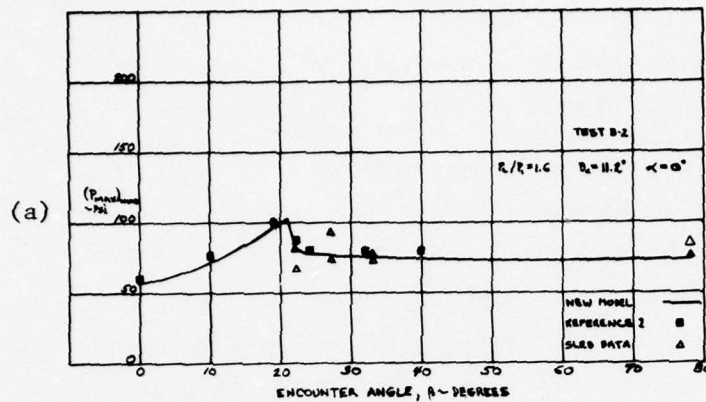
Figure 7. Comparison Between the New Model and
Existing Windward Pressure Data

and, for future reference, it is noted that the pulse duration is
therefore zero. As discussed earlier, the time interval in question
refers to the time it takes for the pressure to decay from the
peak to the quasi-steady level. Therefore, there is no shock-on-
shock pulse over a portion of the leeside of the cone for a portion
of the encounter angle range, and that portion is determined by
comparing the pressure behind the transmitted wave to the leeward
quasi-steady pressure.

The pressure behind the transmitted wave on the leeward ray is
calculated with the wave pattern approximated as shown in Figure 8.
This representation is simpler than that used on the windward ray
and was expected to suffice because there is no transition from
Mach to regular reflection and because of the knowledge gained from
the windward ray analysis at $\beta=0$.
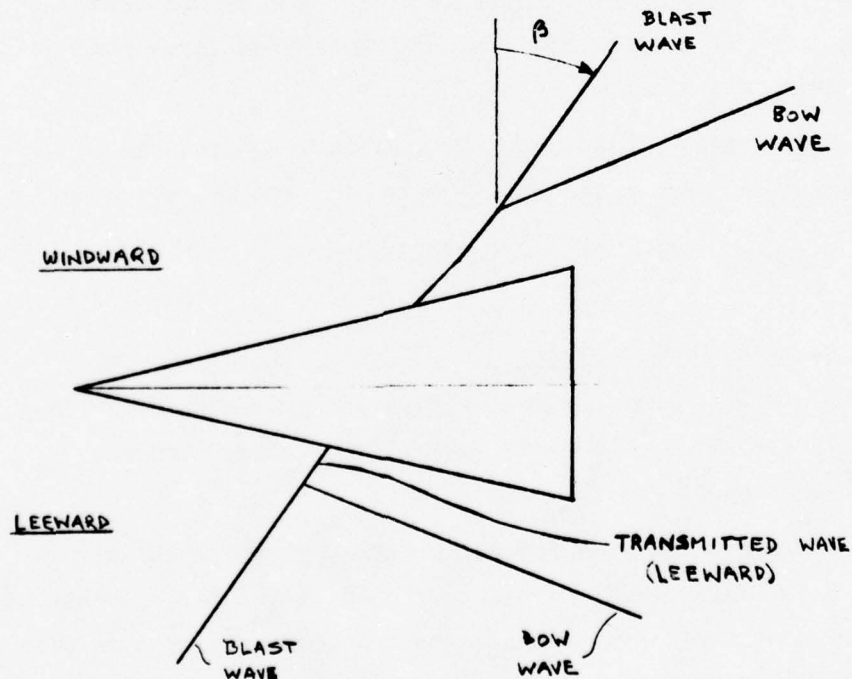
Figure 8. An Approximation to the Leeward Transmitted Shock Wave

The leeward peak pressures calculated with the simpler wave approximation are used to determine the trend with encounter angle as β increases from zero. Non-dimensionalizing the values thus obtained with the value at $\beta=0$ and then using the value calculated at $\beta=0$ with the windward analysis of Section 3.1 produces a good estimate of the leeward pressure behind the Mach stem very conveniently. The leeward analysis proceeds as follows.

The pressure behind the transmitted wave is calculated by again using the Rankine-Hugoniot relations for a normal shock. The assumption that the transmitted wave is straight defines the position and, therefore, the velocity $(V_{Q/W})_{Lee}$ of the point of impingement relative to the body surface as given by the following expression.

$$(V_{Q/W})_{Lee} = V_{B/W} \frac{\cos (\beta-\delta)}{\cos (\beta-\theta_c)} . \qquad (5)$$

The velocity of the Mach stem relative to the gas on the cone surface may then be calculated directly, thereby defining the pressure behind the stem.

The quasi-steady pressure (P_{QS}) is calculated with the following semi-empirical expression which was taken from Reference 13.

$$P_{QS} = P_2 + \frac{1}{2} \rho_2 V_2^2 \cos \gamma \left[(2- \frac{0.46}{M_2^2}) \cos \phi + \frac{0.46}{M_2^2}\right] . \qquad (6)$$

where the quantities P_2, ρ_2, V_2, M_2 are the pressure, density, velocity, and Mach number respectively of the gas behind the blast wave. The angle, γ, is the angle between the velocity vector $\overline{V}_2$ and the outward normal to the cone surface.

Figure 9 shows the peak leeward pressure plotted against encounter angle for several test cases: B-2, B-5 and 6, B-9 and 10. Comparisons with the Kutler results are included, but no test data are presented because of the poor quality of the test data in that region. Agreement between the two methods is seen to be quite good.

22
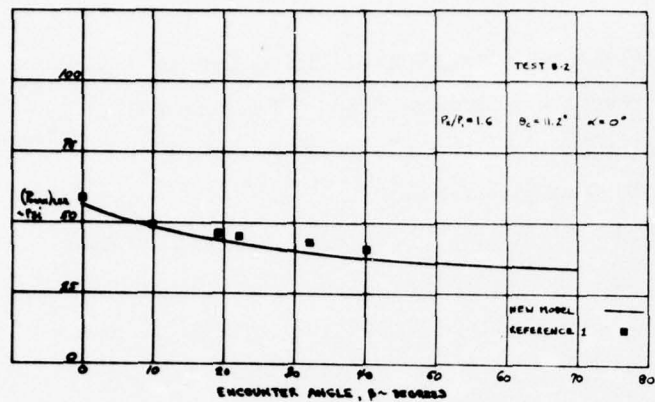
(a)
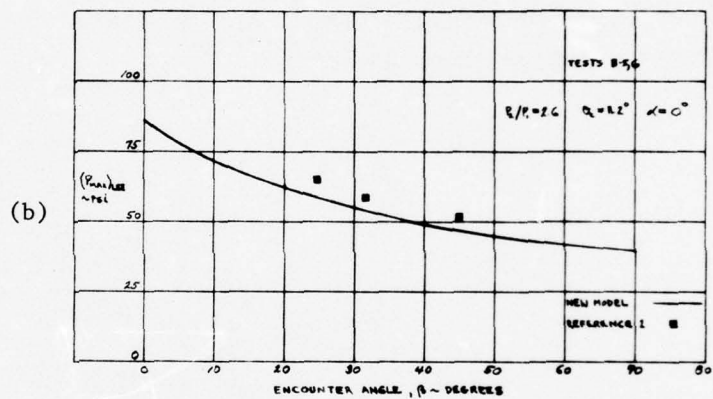
(b)
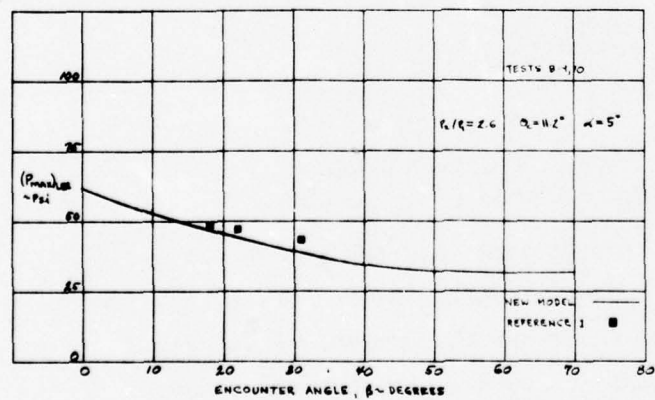
(c)

Figure 9.   Comparison Between the New Model and
Existing Leeward Pressure Data

23

3.3 Windward Pulse Duration

The formulation used to model the duration of the pulse is taken
from an approach suggested by Smyrl (Reference (14). The element of
gas which is at the tip of the cone when the blast arrives, is
flagged and tracked as the wave propagates along the cone. The shock
wave is travelling faster than the disturbed (flagged) gas and so the
distance between them increases with increasing time. The flagged
element of gas is the source of a secondary disturbance which is radi-
ated at the local speed of sound (Figure 10). At any point in time,
the extent to which the second disturbance has radiated, which is
defined by the sonic circle, therefore bounds the region affected by
the propagation shock wave.
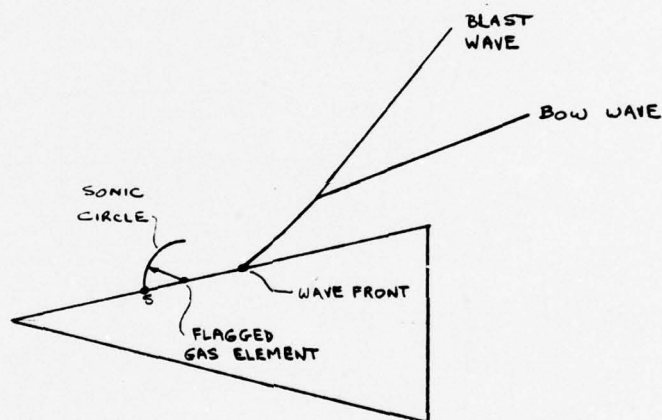
Figure 10. A Model of the Windward
Pulse Duration - Regular Reflection

Smyrl suggested that the time it takes for the pressure to reach
the quasi-steady level can be approximated by the difference in time
between the passage of the wave front and the arrival of the sonic
circle (point S, Figure 10). This reasoning was used and found to
produce excessively large values in comparison to either the Kutler
results or the sled test data. Therefore, the approach was modified

by assuming that the secondary disturbance, namely the one emanating from the flagged gas element, is insignificant and that the quasi-steady pressure is reached when the flagged element passes the point in question. This approach gives much better agreement with the other data and therefore is implemented in the model when regular reflection occurs.

In the Mach reflection regime, this approach was found to give contradictory results in that the pulse duration appeared to decrease with increasing β. The Mach stem produces a stronger disturbance and, thus, the secondary disturbance is probably not insignificant although the duration is still overpredicted if the sonic circle reasoning is used. Therefore, a new model was formulated as follows.

The ratio of the quasi-steady pressure to the pre-encounter surface pressure defines an effective wave front which follows the actual wave front (Figure 11). The speed of the effective wave associated with the quasi-steady pressure level is defined by this pressure ratio and therefore defines an estimate of the arrival of the quasi-steady level of pressure. The pulse duration is approximated by the interval between the arrival of the actual wave front, which is known from the peak pressure analysis of Section 3.1, and the arrival of the effective wave front associated with the quasi-steady pressure.

Figure 12 presents comparisons between the current results, Kutler's calculations, and the sled test data. The figure shows the windward pulse duration plotted against encounter angles for the conditions corresponding to sled tests B-2, B-5 and 6, B-9 and 10 respectively. It should be noted that the Kutler and sled test pulse durations are taken from pressure time traces which approach the quasi-steady value asymptotically, and so the point at which the pulse ends is somewhat subjective and therefore is not always precisely

25

defined. However, the values shown are representative and consistently arrived at and do lend credibility to this simple model.
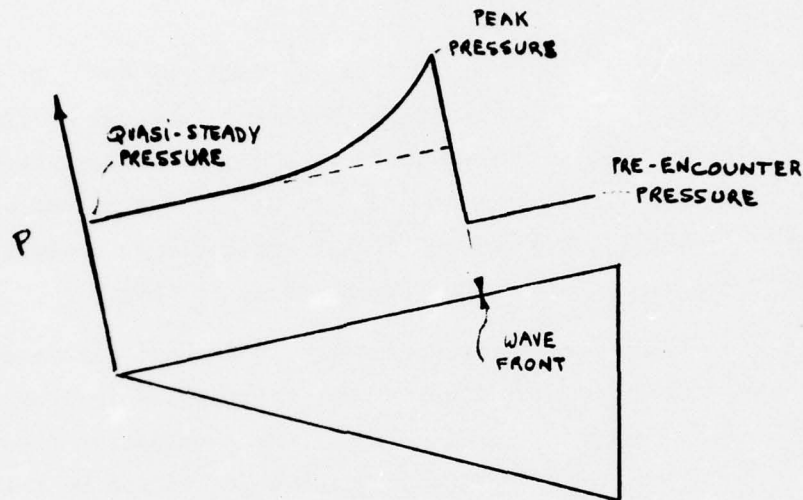
Figure 11. A Model of the Windward
Pulse Duration - Mach Reflection

3.4 Leeward Pulse Duration

A very simple model was chosen for the leeward pulse duration because of the information available from the analyses previously performed. It was noted earlier that the peak leeward pressure at most encounter angles will not exceed the quasi-steady pressure and, therefore, the pulse duration is zero. The encounter angle at which the crossover occurs, labelled earlier as β_{QS}, is typically no larger than about 15 degrees. That is, the leeward pulse duration is non-zero only between $\beta=0$ (nose on) and $\beta=\beta_{QS}$. The pulse duration at $\beta=0$ is already defined by the windward analysis and so the leeward pulse duration is simply assumed to vary linearly with β from the value calculated at $\beta=0$ to zero at $\beta=\beta_{QS}$.
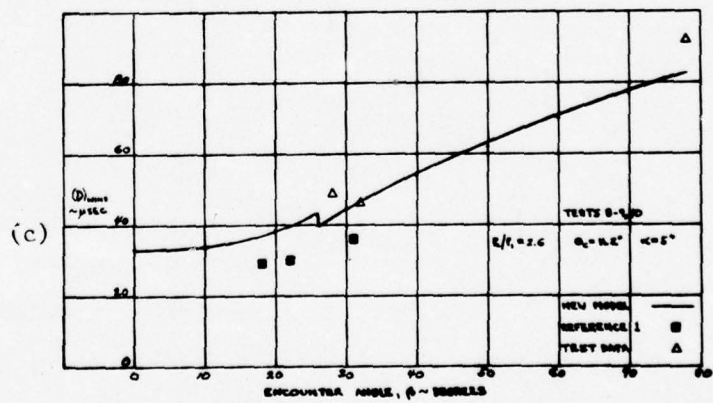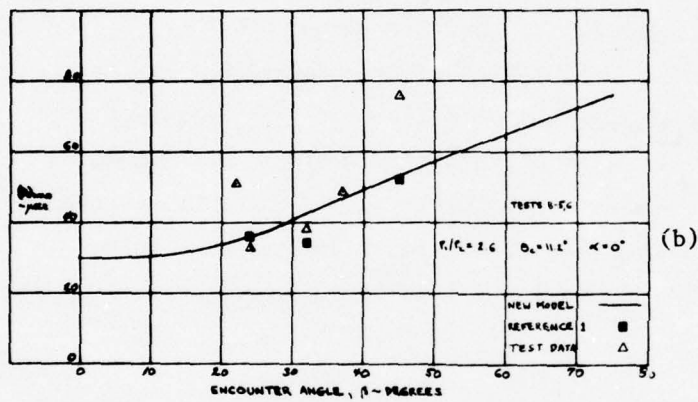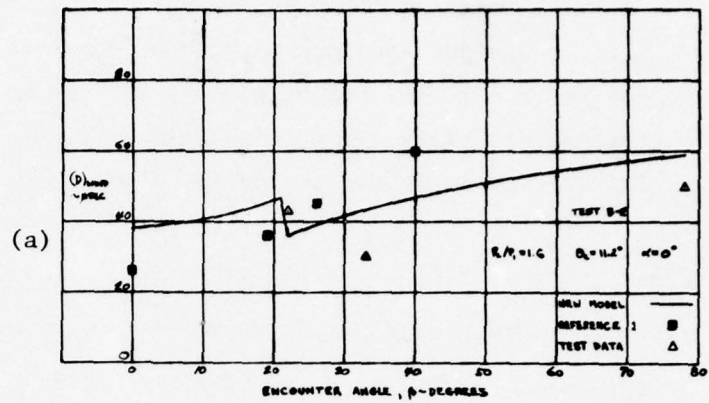
Figure 12. Comparisons Between the New Model and
Existing Windward Pulse Duration Data

27

This approach is illustrated in Figure 13 wherein the durations are plotted against encounter angle for the conditions corresponding to sled tests B-2, B-5 and 6, B-9 and 10. As with the pressures on the leeside, there are no sled test data available and the Kutler results are all at encounter angles beyond $\beta=\beta_{QS}$, and so agreement at $\beta<\beta_{QS}$ cannot be checked. However, over most of the range of encounter angles, where the duration is zero, agreement is established.

3.5 Circumferential Distribution - Peak Pressures

The model of the circumferential distribution of peak pressure uses the information gained from the windward and leeward analyses regarding the position and velocity of the wave front. The assumption is made that the plane defined by the windward and leeward wave front locations (see Figure 14) contains the wave front at all locations around the circumference. The line of intercept between the plane, thus defined, and the cone surface is taken to be the location of the wave front. The wave front location also defines the wave velocity relative to the surface (V_Q) as given by:

$$V_Q = \frac{(1 - K_1)}{\cos \phi - K_1} (V_{Q/W})_{wind} \tag{7}$$

where

$$K_1 = \frac{1 + (V_{Q/W})_{lee}/(V_{Q/W})_{wind}}{1 - (V_{Q/W})_{lee}/(V_{Q/W})_{wind}} \tag{8}$$

$(V_{Q/W})_{wind}$, $(V_{Q/W})_{lee}$ = wave front velocities relative to the surface along the windward and leeward rays respectively.

ϕ = circumferential angle measured in a plane perpendicular to the cone axis with $\phi=0$ at the windward ray.

28
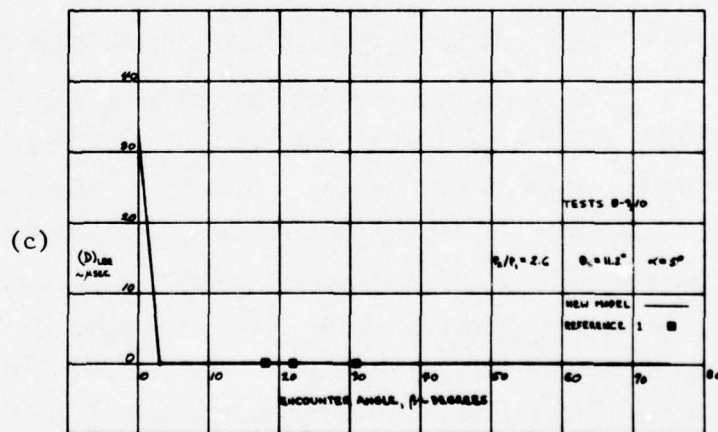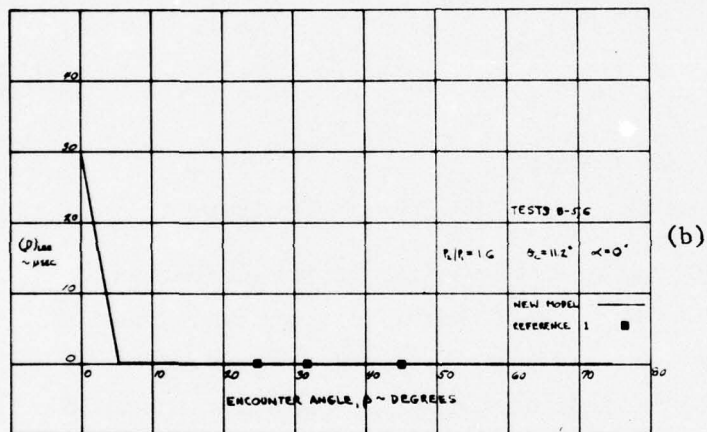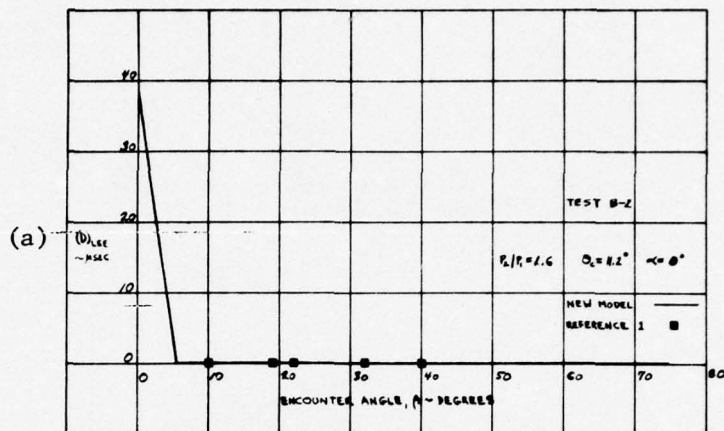
Figure 13. Comparison Between the New Model and
Existing Leeward Pulse Duration Data

29
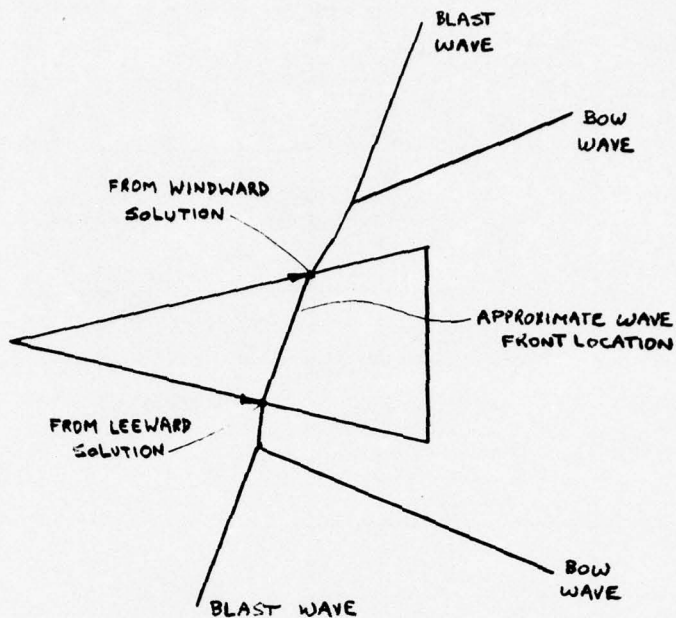
Figure 14. An Approximation to the Wave Front Location

The wave front velocity relative to the gas on the surface in front of the wave may then be calculated which, in turn, determines the wave Mach number and pressure jump by virtue of the Raskine-Hugoniot equations. Since the angle of attack is restricted to small values, the effect of angle of attack on the local flow direction is neglected in computing the velocity of the wave relative to the gas.

It is recognized that the actual wave front will actually curve around the surface so it will not be in a plane as suggested here. However, this model is seen to produce a plausible distribution of peak pressure as evidenced in Figure 15 where the calculated values are plotted against the circumferential angle, ϕ. The values obtained by Kutler and those measured during the sled tests are also shown. Again, the comparisons are presented for the B-2, B-5 and 6, B-9 and 10 test conditions, and reasonable agreement is achieved between Kutler's results and the current model.
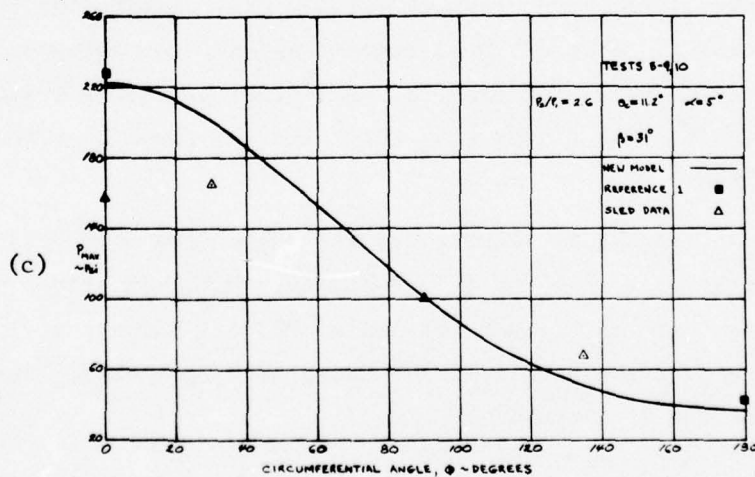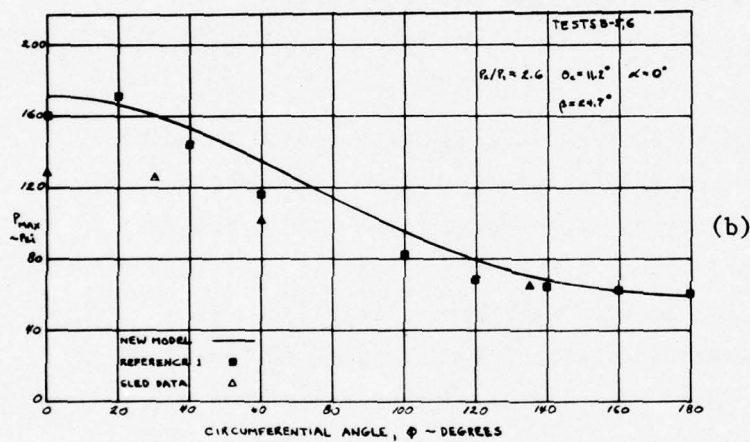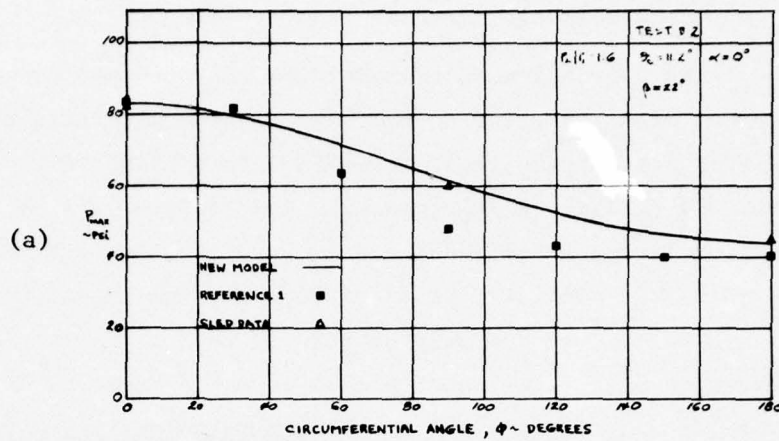
Figure 15. Comparisons Between the New Model and Existing
Circumferential Pressure Data

3.6 Circumferential Distribution - Pulse Duration

The approach used to model the windward and leeward pulse durations
is not easily applied to the circumferential distribution because of the
difficulty in modeling the surface streamlines of the flowfield behind
the blast wave. On the windward and leeward rays of the cone, the
streamlines are defined because they coincide with the geometric
rays of the cone. At other circumferential locations, the stream-
lines are curved not only because of the initial angle of attack,
but also because of the angle of attack induced by the blast wave.
Thus, attempting to follow a flagged element of gas cannot be
achieved without solving for the entire flow field because the path is
not known.

An approach is taken which is analogous to that used to model
the circumferential distribution of peak pressures (see Section 3.5).
It is recalled that the location of the wave front around the cir-
cumference is approximated by the surface intercept of the plane
defined by the windward and leeward wave front locations. In a
similar manner, the windward and leeward locations of the quasi-
steady region define a plane. The surface intercept of that plane
around the circumference defines an approximation to the circumferen-
tial location of quasi-steady region. The pulse duration at any cir-
cumferential location, ϕ, is defined as the time interval between
the passage of the wave front and the passage of the quasi-steady
"front."

Figure 16 illustrates the use of the above reasoning in sled
tests B-2, B-5 and 6, B-9 and 10. Pulse durations are plotted
against the circumferential angle, ϕ. Unfortunately, no other
results are available for comparison from either the Kutler solution
or the sled tests.

32
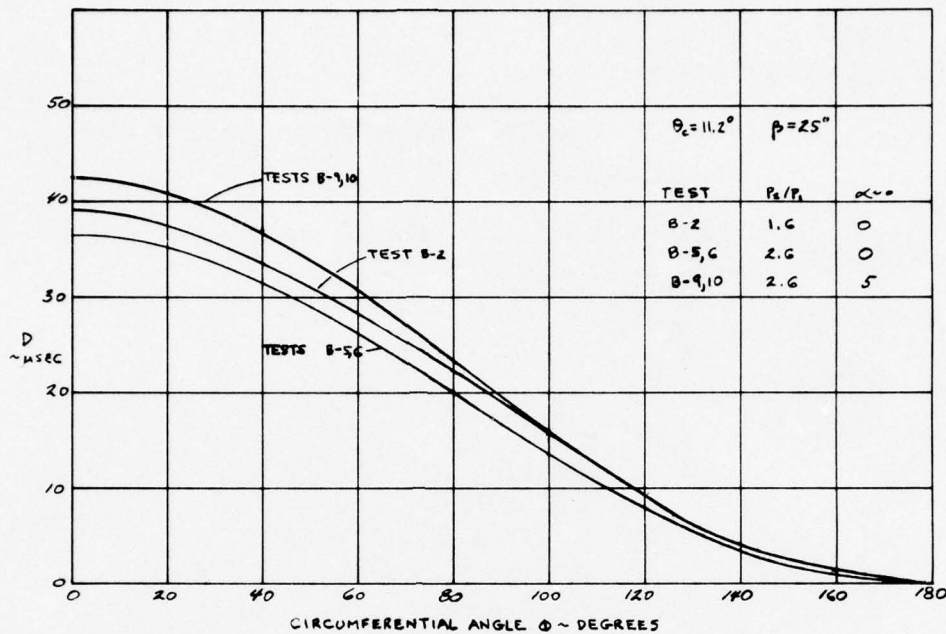
Figure 16. Typical Distributions of Pulse Duration

3.7 Engulfment Time

An additional feature of the phenomenon which is of interest
to the structural dynamist is defined as the engulfment time. This
quantity pertains to the passage of the wave front over a particular
axial station of the body. In general, the wave front reaches the
subject station first on the windward ray and last on the leeward
ray. The differential time between the first and last arrival is
called the engulfment time and it influences the manner in which the
energy is propagated into the structure. Obviously, engulfment time
is easily calculated from the results produced with the foregoing
analysis because the speed of the wave front was defined at the
windward and leeward rays. Therefore, the engulfment time (ENGTIM)
at axial station X is given by

$$(E)_{TIM} = \frac{10^6 X}{\cos \theta_c} \left[\frac{1}{(V_{Q/W})_{lee}} - \frac{1}{(V_{Q/W})_{wind}} \right] \tag{9}$$

33

where

θ_c = cone half-angle

$(V_{Q/W})_{lee}$ = wave front velocity relative to the cone along the leeward ray.

$(V_{Q/W})_{wind}$ = wave front velocity relative to the cone along the windward ray.

4.0 COMPUTER PROGRAM

The analysis described in the foregoing sections was programmed
on Martin Marietta's IBM 370/158 computer. The analysis was programmed
using FORTRAN IV through a time sharing terminal system. The following
paragraphs describe the structure, input/output features, a complete
listing of the program, and a sample problem.

4.1 Program Logic and Structure

The program is designed to analyze the encounter between a super-
sonic sharp cone and a planar blast wave. The cone may be at a small
angle of attack (α) where small is taken to mean less than the cone
half-angle, and the encounter angle (β) may be anywhere from nose-on
to broadside. The only encounter in this range which cannot be treated
is the case where the blast wave is parallel to the bow wave. This
is not a serious matter because the solution is well behaved at smaller
and larger angles and is relatively insensitive to encounter angles in
that regime.

The program is set up to automatically cover the entire range of
encounter angles from nose-on to broadside with a predetermined incre-
ment of 5 degrees. This arrangement was chosen because the angle at
which the peak pressure is highest cannot be determined a priori. Since
the cost of running the program is small, the user is therefore en-
couraged to allow the program to find the worst condition by covering
the entire range. Since there is a discontinuity in the peak pressure
at the encounter angle, where transition from regular to Mach reflection
occurs, the program then proceeds to perform the calculation at 1-degree
intervals in the vicinity of the discontinuity to reduce the likeli-
hood of missing the peak.

At each encounter angle, the windward peak pressure and pulse duration are calculated first followed by the analogous calculations on the leeward ray of the cone. The circumferential distributions are then evaluated and printed out.

The analysis is performed at an axial station (X) selected by the user. The station does not affect the pressure calculation because the flow field is presumed to be independent of physical scale and that the wave pattern remains self-similar as it moves down the body. The pulse duration, on the other hand, does vary with the scale of the problem because it is determined by the time required to traverse a physical distance.

Figure 17 is a flow chart for the total program. The initial decision point pertains to the encounter angle range of interest followed by a choice of branches for zero and non-zero angle of attack. Three major paths are identified by the index K. The first (K=1) treats the case of $\beta=0$ for the leeward ray of a cone at angle of attack. The cone at angle of attack is treated as an effective cone at zero α with cone angles equal to $\theta_c + \alpha$ and $\theta_c - \alpha$, respectively, at the windward and leeward rays. At $\beta=0$, using the leeward ray flow conditions and the windward ray analysis, the peak pressure and pulse duration are calculated and stored for later use in the leeward analysis at $\beta\neq0$. If $\alpha=0$, the path K=1 is omitted.

The path K=2 treats the complete encounter angle range from nose-on to broadside. The sequence begins with the analysis of the windward ray followed by the leeward ray and finally the circumferential distribution. The sequence is initialized with the local flow conditions on the real or effective cone depending on whether or not the angle of attack is zero.

The path K=3 treats four additional encounter angles in the vicinity of the value of β at which transition from Mach to regular

36

reflection occurs. In this way, local peak in pressure which occurs at the transition point is well defined.
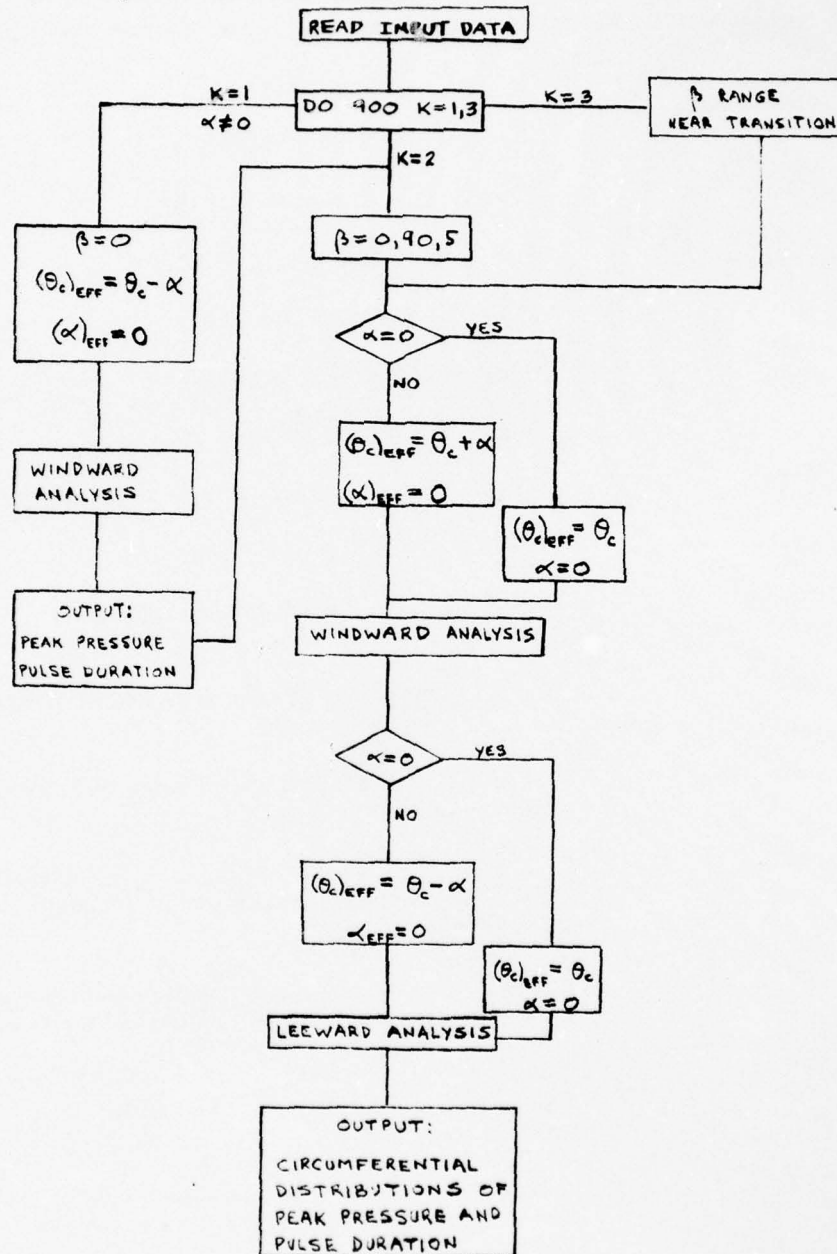
Figure 17. Total Program Flow Chart

37

4.2 Input/Output

Input

The following twenty quantities must be input to run the program.

Program Symbol	Definition
N	Number of blast strengths
P1	Freestream pressure, $\#/in^2$
R1	Freestream density, $\#/ft^3$
V1	Freestream velocity, ft/s
TC	Cone semi-vertex angle, deg
ALD	Angle of attack, deg
P2P1	Blast pressure ratio, non-dimensional
TWOD	Bow wave angle, $\alpha=0$, deg
PWP1O	Cone surface-to-freestream pressure ratio, $\alpha\neq0$, non-dimensional
RWR1O	Cone surface-to-freestream density ratio, $\alpha=0$, non-dimensional
V3WO	Flow velocity at cone surface relative to the cone, $\alpha=0$, ft/s
TWLEED	Leeward ray bow wave angle, $\alpha\neq0$, measured from the effective cone centerline (Figure 4), deg
PWP1LE	Cone surface-to-freestream pressure ratio on the leeward ray, $\alpha\neq0$, non-dimensional
RWR1LE	Cone surface-to-freestream density ratio on the leeward ray of the cone, $\alpha\neq0$; non-dimensional
V3WLEE	Flow velocity on the leeward ray of cone ray surface relative to the cone, $\alpha\neq0$, ft/s

38

TWWD	Windward ray bow wave angle, $\alpha \neq 0$, measured from the effective cone centerline (Figure 15), deg
PWP1W	Cone surface-to-freestream pressure ratio on the windward ray, $\alpha \neq 0$, non-dimensional
RWR1W	Cone surface-to-freestream density ratio on the leeward ray, $\alpha \neq 0$, non-dimensional
VW	Flow velocity on the windward ray of cone surface relative to the cone, ft/s
X	Axial station at which the analysis is performed, ft.

The input format for the above quantities for the usual batch processing on a computer is as follows. The sequence of inputs, as presented, must be adhered to but there is no other format restriction other than the total number of quantities on each card.

Card	Input Quantities
1	N, P1, R1, V1, TC, ALD, P2P1
2	TWOD, PWP1O, RWR1O, V3WO, TWLEED, PWP1LE, RWR1LE
3	V3WLEE, TWWD, PWP1W, RWR1W, VW, X

Output

The output information (an example of which is presented in Section 4.4) summarizes some of the input data and contains the circumferential distributions of peak pressure and pulse duration at each of the encounter angles.

The input quantities printed out are the cone semi-vertex angle, freestream velocity, angle of attack, axial station, and blast pressure ratio. At each encounter angle (β) that the analysis is performed, beginning with zero, the quantity printed first is the engulfment time (μs) followed by the distribution of pre-encounter pressure, peak shock-on-shock pressure, quasi-steady pressure, and

pulse duration with circumferential body angle ϕ. It is recalled that $\phi=0$ corresponds to the windward ray. All pressures are in psi and the pulse duration is given in μs.

4.3 Program Listing

A listing of the computerized shock-on-shock model is given in the following pages. For the benefit of the user and/or programmer, a number of comments are included in the listing. The comments spell out the input quantities required to run the program, to identify major subsections of the analysis, and to define key variables.

4.4 Sample Problem

A sample problem was run to demonstrate the output format and to provide a check case. The example employs the conditions corresponding to sled tests B-9 and B-10 as listed below.

Quantity	Value	Quantity	Value
N	1	V3WO	5426.0 ft/s
P1	12.6 psi	TWLEED	13.0 deg
R1	0.0627 lb/ft^3	PWP1LE	1.69
V1	5500 ft/s	RWR1LE	1.396
TC	11.2 deg	V3WLEE	5584.0 ft/s
ALD	5.0 deg	TWWD	20.6 deg
P2P1	2.6	PWP1W	3.93
TWOD	16.6 deg	RWR1W	2.508
PWP10	2.596	VW	5375.0 ft/s
RWR10	1.95	X	1.25 ft

To reduce the volume of paper, the program was modified to produce results only at four encounter angles: 0, 20, 40, and 60 degrees. The output is presented on the facing page.

SIMPLIFIED SHOCK-ON-SHOCK MODEL

CONE HALF-ANGLE= 11.20   CONE VELOCITY= 5500.00   ANGLE OF ATTACK= 5.00
AXIAL STATION=   1.25   BLAST STRENGTH= 2.60

BETA= 0.0

ENGULFMENT TIME(MICRO-SEC)=   0.0

CIRCUMFERENTIAL ANGLE,PHI-DEG	PRE-ENCOUNTER PRESSURE-PSI	PEAK PRESSURE PSI	QUASI-STEADY PRESSURE-PSI	PULSE DURATION MICRO-SEC
0.0	49.52	128.43	117.98	33.06
20.00	48.67	126.29	115.38	32.24
40.00	46.22	120.21	108.12	29.85
60.00	42.46	111.11	97.64	26.18
80.00	37.86	100.28	85.85	21.66
100.00	32.96	89.17	74.58	16.83
120.00	28.35	79.11	65.20	12.28
140.00	24.60	71.17	58.42	8.55
160.00	22.15	66.11	54.41	6.12
180.00	21.29	64.37	53.09	5.27

BETA=20.00

ENGULFMENT TIME(MICRO-SEC)= 17.58

CIRCUMFERENTIAL ANGLE,PHI-DEG	PRE-ENCOUNTER PRESSURE-PSI	PEAK PRESSURE PSI	QUASI-STEADY PRESSURE-PSI	PULSE DURATION MICRO-SEC
0.0	49.52	223.69	145.19	38.85
20.00	48.67	215.26	140.42	37.55
40.00	46.22	192.33	127.25	33.88
60.00	42.46	160.83	108.74	28.40
80.00	37.86	127.64	88.76	21.89
100.00	32.96	98.20	70.81	15.20
120.00	28.35	75.39	57.05	9.14
140.00	24.60	59.87	48.06	4.36
160.00	22.15	51.08	43.27	1.30
180.00	21.29	48.26	41.81	0.25

BETA=40.00

ENGULFMENT TIME(MICRO-SEC)= 23.11

CIRCUMFERENTIAL ANGLE,PHI-DEG	PRE-ENCOUNTER PRESSURE-PSI	PEAK PRESSURE PSI	QUASI-STEADY PRESSURE-PSI	PULSE DURATION MICRO-SEC
0.0	49.52	219.97	169.78	52.87
20.00	48.67	210.29	162.79	51.04
40.00	46.22	184.26	143.68	45.88
60.00	42.46	149.29	117.33	38.23
80.00	37.86	113.58	89.84	29.23
100.00	32.96	83.11	66.45	20.09
120.00	28.35	60.48	49.98	11.89
140.00	24.60	45.71	40.50	5.47
160.00	22.15	37.63	36.22	1.39
180.00	21.29	35.09	35.09	0.0

BETA=60.00

ENGULFMENT TIME(MICRO-SEC)= 25.13

CIRCUMFERENTIAL ANGLE,PHI-DEG	PRE-ENCOUNTER PRESSURE-PSI	PEAK PRESSURE PSI	QUASI-STEADY PRESSURE-PSI	PULSE DURATION MICRO-SEC
0.0	49.52	225.63	186.64	68.01
20.00	48.67	215.23	177.89	65.64
40.00	46.22	187.37	154.10	58.94
60.00	42.46	150.23	121.77	49.02
80.00	37.86	112.71	88.90	37.40
100.00	32.96	81.09	62.13	25.66
120.00	28.35	57.94	44.68	15.16
140.00	24.60	43.04	35.99	6.96
160.00	22.15	34.98	33.00	1.77
180.00	21.29	32.46	32.46	0.0

1

```
00001 C      SIMPLIFIED SHOCK-ON-SHOCK MODEL
00002 C
00003 C      INPUT QUANTITIES
00004 C
00005 C      N=NUMBER OF BLAST STRENGTHS      P1=FREESTREAM PRESSURE,LB/IN2
00006 C      R1=FREESTREAM DENSITY,LB/FT3     V1=FREESTREAM VELOCITY,FT/SEC
00007 C      TC=CONE SEMI-VERTEX ANGLE,DEG.   ALD=ANGLE OF ATTACK,DEG.
00008 C      P2P1=BLAST PRESSURE RATIO,NON DIM.
00009 C      TWOD=BOW WAVE ANGLE,ALD=0,DEG.
00010 C      PWP1O=CONE-TO-FREESTREAM PRESSURE RATIO,ALD=0,NON DIM
00011 C      R4R1O=CONE-TO-FREESTREAM DENSITY RATIO,ALD=0,NON DIM
00012 C      V3WO=FLOW VELOCITY AT CONE SURFACE REL. TO CONE ,ALD=0,FT/SEC
00013 C      TWLEED=LEEWAED RAY BOW WAVE ANGLE,ALD=0,SEE FIG. 15
00014 C      PWP1LE=CONE-TO-FREESTREAM PRESSURE RATIO,LEEWARD RAY,ALD.NE.O,NON
00015 C      DIM
00016 C      RWR1LE=CONE-TO-FREESTREAM DENSITY RATIO,LEEWARD RAY,ALD.NE.O,NON
00017 C      DIM
00018 C      V3WLEE=FLOW VELOCITY,LEEWARD RAY,REL. TO CONE,ALD.NE.O,FT/SEC
00019 C      TWWD=WINDWARD RAY BOW WAVE ANGLE,ALD.NE.O,SEE FIG. 15,DEG.
00020 C      PWP1W=CONE-TO-FREESTREAM PRESSURE RATIO,WINDWARD RAY,ALD.NE.O,NON
00021 C      DIM
00022 C      RWR1W=CONE-TO-FREESTREAM DENSITY RATIO,WINDWARD RAY,ALD.NE.O,NON
00023 C      DIM
00024 C      VW=FLOW VELOCITY,WIND. RAY,REL. TO CONE,ALD.NE.O,FT/SEC
00025 C      X=AXIAL STATION AT WHICH ANALYSIS IS PERFORMED
00026 C
00027 C
00045        DIMENSION P2P2(5),P4P3(2),TBAR(2),THET4(2),THET5(2)
00050        P1=12.6
00070        R1=32.2*0.0019467
00090        V1=5500.
00110        TC=11.2
00130        ALD=5.
00140        TWOD=16.6
00150        PWP1O=2.596
```

```
00170       RARIU=1.95
00190       V3NU=5426.
00210       TWLEED=13.
00230       P4P1LE=1.69
00250       RWR1LE=1.396
00270       V3WLEE=5584.
00290       TWWD=20.6
00310       P4P1W=3.93
00330       RWR1W=2.508
00350       VW=5375.
00370       X=1.25
00410       TCR=TC/57.3
00412       P2P2(1)=2.6
00414       P2P2(2)=1.6
00416       N=1
00430       TWLEE=TWLEED/57.3
00450       TWW=TWWD/57.3
00451 C     N LOOP, NUMBER OF BLAST STRENGTHS TO BE RUN
00452       DO 901 NN=1,N
00454       P2P1=P2P2(N)
00560       WRITE(6,31)
00562    31 FORMAT(//42X,'SIMPLIFIED SHOCK-ON-SHOCK MODEL')
00564       WRITE(6,33)TC,V1,ALD,X,P2P1
00566    33 FORMAT(//5X,'CONE HALF-ANGLE=',F6.2,5X,'CONE VELOCITY=',F9.2
00568      *,5X,'ANGLE OF ATTACK=',F6.2,/5X,'AXIAL STATION=',F7.2,5X,'BLAST ST
00569      *RENGTH=',F6.2)
00580       IF(ALD.LE.TC) GO TO 1
00582       WRITE(6,2)
00590     2 FORMAT(2X,'*** ALPHA-LARGER-THAN-CONE-HALF-ANGLE***')
00610       GO TO 901
00630     1 CONTINUE
00631 C     A1,AM1=SPD OF SND,MACH NO. IN REGION 1
00650       A1=SQRT(32.2*144*1.4*P1/R1)
00670       AM1=V1/A1
00710       P2P1=2.6
00790       AMB=SQRT((6*P2P1+1)/7)
```

43

```
00010        R2R1=(6*AMB**2)/(5.+AMB**2)
00030        A22=P2P1*A1**2/R2R1
00050        VB=AMB*A1
00070        KST$K=0
00390        KCHECK=0
00395        AL=ALD/57.3
00396  C     K SETS RANGE OF ENCOUNTER ANGLE AND ANALYSIS SEQUENCE
00910        DO 900 K=1,2
00930        IF(K.EQ.2) GO TO 26
00950        IF(K.EQ.3) GO TO 27
00955        IF(ALD.EQ.0) GO TO 900
00956  C     K=1,BETA=0,USE WIND. RAY ANALYSIS ON LEESIDE OF CONE AT ALD
00957  C     NOT EQUAL 0
00990        THETCR=TCR-ALD/57.3
00995        THETIC=THETCR*57.3
01010        THETWR=TWLEE
01015        THETW=THETWR*57.3
01030        PWP1=PWP1LE
01050        RWR1=RWR1LE
01070        V3WWT=V3WLEE
01075        A3W2=PWP1*A1**2/RWR1
01090        JB1=1
01110        JB2=1
01130        JBD=0
01150        ALPHA=0
01155        ALPHAD=0
01170        GO TO 21
01190  C     K=2,BETA=0,90,5---WINDWARD,LEEWARD AND CIRCUM DIST ANALYSES
01192  C     INITIALIZE FOR WINDWARD ANALYSIS---ALD NOT ZERO
01210  26    THETCR=TCR+ALD/57.3
01230        THETWR=TWW
01235        THETIC=THETCR*57.3
01240        THETW=THETWR*57.3
01250        PWP1=PWP1W
01270        RWR1=RWR1W
01290        V3WWT=VW
```

44

```
01295          A3N2=PHP1*A1**2/RWR1
01310          J31=1
01330          J32=91
01350          J3D=20
01355          ALPHAD=ALD
01356 C        RE-INITIALIZE IF ALD EQUAL ZERO
01357          ALPHA=ALD/57.3
01358          IF(ALD.NE.0) GO TO 21
01359          THETCR=TCR
01360          THETC=TCR*57.3
01361          THETA=TWD
01362          THETAR=TWOD/57.3
01363          PHP1=PHP10
01364          R.R1=RWR10
01365          V3WT=V3WU
01367          A3N2=PHP1*A1**2/RWR1
01370          GO TO 21
01392 C        K=3, SET BETA RANGE NEAR TRANSITION,REPEAT COMPLETE ANALYSIS
01410 27       J31=BSTEM+2
01430          J32=BSTEM+5
01450          J3D=1
01470          KSTEM=0
01490 21       CONTINUE
01510          PHP1=.95*PHP1
01530          THETA=(THETA+THETC)/2
01550          AM1ST=V1*SIN(THETAR)/A1
01570          P3P1=(7*(AM1ST**2)-1)/6
01590          U34W=V3WT*COS(THETCR)
01610          V3WW=-V3WT*SIN(THETCR)
01611 C        ENCOUNTER ANGLE(BETA) LOOP
01630          DO 302 J3=J31,J32,JBD
01650          BETAD=J3-1
01670          BETA=BETAD/57.3
01690          BE=BETA-ALPHA
01710          BED=BE*57.3
01730          BCR=19.
```

```
01750        IF((90-BED).LE.THETC) GO TO 802
01752        IF(K.EQ.1)GO TO 42
01770   23   WRITE(6,17)BETAD
01790   17   FORMAT(/42X,'BETA=',F5.2)
01792   42   CONTINUE
01810        BEDJD=90.-THETA
01830        BBUM=BBUAD/57.3
01850        IF(BED.NE.BBUND) GO TO 12
01870        WRITE(6,11)
01890   11   FORMAT(2X,'NO SOLUTION-BLAST PARALLELS BOW WAVE')
01910        GO TO 802
01930   12   CONTINUE
01950        ANGLE=90-(BE+THETWR)*57.3
01970        AMDSB=AMD*SIN(BE)
01990        UBW=VB*COS(BE)+V1
01991   C     VELOCITIES(V) AND FLOW DIRECTIONS(THET) ARE LABELLED BY FLOW
01992   C     FIELD REGION, E.G., V2W=Y COMP. OF VEL. IN REGION 2 REL TO CONE(W)
01993   C     V2WT=TOTAL VEL IN REGION 2,REL. TO CONE
01994   C     THETA=FLOW DIRECTION IN REGION 4 REL. TO BODY FIXED X AXIS
02030        VBW=VB*SIN(BE)
02050        VBWT=(UBW*UBW+VBW*VBW)**.5
02070        DEL=ATAN(VBW/UBW)
02090        BMD=BE-DEL
02110        DMB=DEL-BE
02130        BPTW=BE+THETWR
02150        VPWT=VBWT*COS(BMD)/COS(BPTW)
02170        IF(BE.LT.BBDW) GO TO 14
02190        VPWT=-VBWT*COS(DMB)/COS(BPTW)
02210        UPW=-VPWT*COS(THETWR)
02230        VPW=VPWT*SIN(THETWR)
02250        GO TO 13
02270   14   UPW=VPWT*COS(THETWR)
02290        VPW=-VPWT*SIN(THETWR)
02310   13   V2BT=VB-(144*32.2*P1*(P2P1-1.)/(R1*VB))
02330        U2W=(VB-V2BT)*COS(BE)+V1
02350        V2W=(VB-V2BT)*SIN(BE)
```

46

```
02370        VN1W=V1*SIN(THET1P)
02390        VT31=V1*COS(THET1R)
02410        VN31=V11-(((P3P1-1)*12.5*144*32.2)/(R1*VN1W))
02430        GA=ATAN(VN31./VT31)
02450        V3WT=V1*COS(THETWR)/COS(GA)
02470        U3W=V3WT*COS(THETWR-GA)
02490        V3W=-V3WT*SIN(THETWR-GA)
02510  C     VELOCITIES REL TO P(INTERSECTION BETWEEN BOW AND BLAST WAVE)
02530        U1P=V1-UPW
02550        V1P=-VPW
02570        V1PT2=U1P*U1P+V1P*V1P
02590        A1P2=V1PT2/(A1*A1)
02610        U2P=U2W-UPW
02630        V2P=V2W-VPW
02650        V2PT2=U2P*U2P+V2P*V2P
02670        U3P=U3W-UPW
02690        V3P=V3W-VPW
02710        V3PT2=U3P*U3P+V3P*V3P
02730  C     FLOW DIRECTIONS
02750        THET1=ABS(ATAN(V1P/U1P))
02770        IF(BE.LT.BBOW) GO TO 62
02790        AL13=THETWR-THET1
02810        GO TO 63
02811  C     ANGLE AL13 REFERS TO THE WAVE SEPARATING REGIONS 1 AND 3
02812  C     MEASURED BETWEEN FLOW IN REGION 1(THET1) AND THE WAVE
02830  62    AL13=THET1-THETWR
02850  63    AMIS32=AMIP2*SIN(AL13)*SIN(AL13)
02870        CDEL13=(((1.2*AMIP2)/(AMIS32-1))-1)*TAN(AL13)
02890        XCD13=1./CDEL13
02910        DEL13=ATAN(XCD13)
02911  C     ANGLE DEL13 REFERS TO THE CHANGE IN FLOW DIRECTION IN GOING
02912  C     FROM REGION 1 TO REGION 3
02930        IF(BE.LT.BBOW) GO TO 64
02950        THET3=THET1+DEL13
02970        AL12=THET1-90./57.3+BE
02990        GO TO 65
```

```
03010   64 THET3=THET1-DEL13
03030      AL12=90./57.3-(THET1+BE)
03050   65 AM1SA2=AM1P2*SIN(AL12)*SIN(AL12)
03070      CDEL12=(((1.2*AM1P2)/(AM1SA2-1))-1)*TAN(AL12)
03090      XCD12=1./CDEL12
03110      DEL12=ATAN(XCD12)
03130      IF(BE.LT.BBOW) GO TO 66
03150      THET2=THET1-DEL12
03170      GO TO 67
03190   66 THET2=THET1+DEL12
03210   67 A3A12=(7.*AM1P2*(SIN(AL13))**2.-1.)*(AM1P2*(SIN(AL13))**2.+5.)
03230      */(36.*AM1P2*(SIN(AL13))**2.)
03250      A32=A3A12*A1*A1
03270      AM3P2=V3PT2/A32
03290      AM2P2=V2PT2/A22
03310      PUP1=(7.*AM3P2-1.)/6.
03330      PUP2=P2P1*(7.*AM2P2-1.)/(P3P1*6.)
03350      IF(PUP2.GT.PUP1) GO TO 51
03370   50 P4P3UP=PUP2
03390      GO TO 52
03410   51 P4P3UP=PUP1
03430   52 P4P3(2)=P2P1*.95
03431    C
03432    C  CHOUSE(ITERATE) P4P3 SO AS NOT TO EXCEED THEO.LIMITS PUP1
03450    C  OR PUP2
03470      IF(P2P1.LE.P4P3UP)GO TO 59
03490      P4P3(2)=P4P3UP*.95
03510   59 JMAX=P2P1*100000
03530      DO 53 J=1,JMAX
03550      AL34=ASIN(SQRT((6.*P4P3(2)+1.)/(7.*AM3P2)))
03570  998 AM3SA2=AM3P2*SIN(AL34)*SIN(AL34)
03590      CDEL34=(((1.2*AM3P2)/(AM3SA2-1))-1)*TAN(AL34)
03610      XCD34=1./CDEL34
03630      DEL34=ATAN(XCD34)
03650      IF(BE.LT.BBOW) GO TO 68
03670      THET4(2)=THET3-DEL34
           GO TO 69
```

```
03690      63 THET4(2)=THET3+DEL34
03710      69 V4V32=1.-(5./35.)*(AM3SA2-1.)*(7.*AM3SA2+5.)/(AM3P2*AM3SA2)
03730         V4PT2=V4V32*V3PT2
03750         P3P2=P3P1/P2P1
03770         P5P2=P4P3(2)*P3P2
03790         AL52=ASIN((6.*P5P2+1.)/(7.*AM2P2))**.5
03810         AM2SA2=AM2P2*SIN(AL52)*SIN(AL52)
03830         CDEL52=(((1.2*AM2P2)/(AM2SA2-1.))-1)*TAN(AL52)
03850         XCD52=1./CDEL52
03870         DEL52=ATAN(XCD52)
03890         IF(BE.LT.BBUR) GO TO 80
03910         THET5(2)=THET2+DEL52
03930         GO TO 81
03950      80 THET5(2)=THET2-DEL52
03970      81 V5V22=1.-5./36.*(AM2SA2-1.)*(7.*AM2SA2+5.)/(AM2P2*AM2SA2)
03990         V5PT2=V5V22*V2PT2
04010 C    EXAMINE DIFFERENCE IN FLOW DIRECTIONS(TBAR) BET. REGIONS
04011 C    4 AND 5. IF ACCEPTABLE GO TO 4.
04012 C    ADJUSTMENTS TO P4P3 DEPENDS ON SIGN AND SLOPE OF TBAR
04030         TBAR(2)=THET5(2)-THET4(2)
04050         IF(ABS(TBAR(2)).LE.0.00005) GO TO 4
04070         IF(J.GT.1) GO TO 54
04090         P4P3(1)=P4P3(2)
04110         P4P3(2)=P4P3(2)-0.02
04130         TBAR(1)=TBAR(2)
04150         GO TO 53
04170      54 DTDP=(TBAR(2)-TBAR(1))/(P4P3(2)-P4P3(1))
04190         IF(J.GT.2) GO TO 32
04210         B=TBAR(2)-P4P3(2)*DTDP
04230         P4P3(2)=-B/DTDP
04250         IF(P4P3(2).LE.1.0) GO TO 57
04270         GO TO 53
04290      32 IF(BE.GT.45./57.3) GO TO 57
04310         IF(ABS(DTDP).LE.0.0001) GO TO 4
04330      57 IF(TBAR(2).GT.0.0.AND.DTDP.GT.0.0) GO TO 55
04350         IF(TBAR(2).GT.0.0.AND.DTDP.LT.0.0) GO TO 56
```

```
04370        IF(TBAR(2).LT.0.0.AND.DTDP.GT.0.0) GO TO 56
04390        IF(TBAR(2).LT.0.0.AND.DTDP.LT.0.0) GO TO 55
04410   55   P4P3(1)=P4P3(2)
04430        P4P3(2)=P4P3(2)-0.00001
04450        TBAR(1)=TBAR(2)
04470        GO TO 53
04490   56   P4P3(1)=P4P3(2)
04510        P4P3(2)=P4P3(2)+0.00001
04530        TBAR(1)=TBAR(2)
04550        GO TO 53
04570   53   CONTINUE
04590        GO TO 900
04610    4   CONTINUE
04611 C     BLAST-BOW WAVE INTERSECTION SOLVED
04630        IF(BE.LT.BBOW) GO TO 70
04650        EIR=THET3-AL34
04670        EI=EIR*57.3
04690        GO TO 71
04710   70   EIR=THET3+AL34
04730        EI=EIR*57.3
04750   71   CONTINUE
04791 C     IF BETA IS BETWEEN (90-THET?) AND (90-THETC),ASSUME TRANS.
04792 C     WAVE IS UNAFFECTED BY SHOCK LAYER AND OMIT INNER SEG. SOL.
04793 C     SOLUTION OF INNER SEG. OF THE TRANS. WAVE IS BEGUN AT 105
04810        IF(BE.LT.BBOW) GO TO 105
04830        IF(EI.LT.THETC) GO TO 105
04850        AMT32=(6.*P4P3(2)+1.)/7.
04870        VT3T=SQRT(AMT32)*SQRT(A3W2)
04890        UT3=VT3T*SIN(EIR)
04910        VT3=VT3T*COS(EIR)
04930        UTR=UT3+U3W4
04950        VTR=VT3+V3W4
04970        VTRT2=(UTR*UTR+VTR*VTR)
04990        VTRT=SQRT(VTRT2)
05010        Y=ATAN(VTR/UTR)
05030        VONT2=VTRT*SIN(EIR+Y)/SIN(EIR-THETCR)
```

```
05050        UOW=VOW/2*COS(THETCR)
05070        VOW=-VOW/2*SIN(THETCR)
05090        U3O=U3W-UOW
05110        V3O=V3W-VOW
05130        AM3O2=(U3O*U3O+V3O*V3O)/A3W2
05150        P4P3IN=P4P3(2)
05170        AL34W=E1R-THETCR
05190        SAL34W=SIN(AL34W)*SIN(AL34W)
05210        GO TO 101
05230 C *****DEFINE CONDITIONS IN INNER LAYER
05231 C      P4OUT=PRESSURE AT MATCH POINT(R) BEHIND THE OUTER SEGMENT
05232 C      OF THE TRANS. WAVE, P4IN=CORRESP. PRESSURE FOR INNER SEGMENT
05250 105    P4OUT=P4P3(2)*PWP1*P1
05270        THETU=THETM
05290        IF(BED.GT.BCR) GO TO 83
05310        THETU=.99*THETM+BETAD*(THETM-.99*THETM)/BCR
05330 83     THETUR=THETU/57.3
05350        IF(BE.LT.BBOW )GO TO 72
05370        E2=-90.
05390        GO TO 73
05410 72     E2=THETU
05430 73     L=0
05450        DO 700 N=1,180
05470        E2=E2+1.
05490 84     E2R=E2/57.3
05510        E1MIN=E1R-THETMR
05530        E1MID=E1R-THETOR
05550        VRAT=VPAT*SIN(E1MTH)/SIN(E1MTU)
05570        E2MTU=E2R-THETUR
05590        E21RC=E2R-THETCR
05610        VOWT2=VRAT*SIN(E2MTU)/SIN(E2MTC)
05630        IF(BE.LT.BROW) GO TO 75
05650 100    UOWT2=-VOWT2*COS(THETCR)
05670        VOW2=VOW/2*SIN(THETCR)
05690        GO TO 76
05710 75     UOW2=VOW/2*COS(THETCR)
```

```
05730        V3W2=-V0WT2*SIN(THETCR)
05750   76   U3Q=U3WW-U0W2
05770        V3Q=V3WW-V0W2
05790        AM3Q2=(U3Q*U3Q+V3Q*V3Q)/A3W2
05810        AM3Q=SQRT(AM3Q2)
05830   C    CALCULATE INNER SEGMENT PRESSURE
05850   77   AL34W=E2R-THETCR
05870   78   SAL34W=SIN(AL34W)*SIN(AL34W)
05890        P4P3IN=(7.*AM3Q2*SAL34W-1.)/6.
05910        P4IN=P4P3IN*PMP1*P1
05911   C    EXAMINE DIFFERENCE(DP) BETWEEN P4OUT AND P4IN, WHEN ACCEPT.
05912   C    THEN INNER SEGMENT IS DEFINED
05930        DP=P4IN-P4OUT
05950        IF(ABS(DP).LE.0.01) GO TO 701
05970        IF(BE.LT.BBOW).GO TO 74
05990        IF(DP.GT.0.0) GO TO 700
06010        E2=E2-0.0001
06030        L=L+1
06050        IF(L.GE.10000) GO TO 701
06070        GO TO 84
06090   74   IF(DP.LT.0.0) GO TO 700
06110        E2=E2-0.0001
06130        L=L+1
06150        IF(L.GE.10000) GO TO 701
06170        GO TO 84
06190   700  CONTINUE
06210   701  CONTINUE
06230   C    INNER SEGMENT OF TRANS. WAVE DEFINED,NOW DETERMINE IF
06232   C    REGULAR REFLECTION AT SURFACE IS POSSIBLE BY FINDING
06234   C    REFLECTED WAVE ANGLE AL46
06330   101  AM4Q2=(AM3Q2*(6.*P4P3IN+1.)-5.*(P4P3IN**2-1.)/(P4P3IN*(P4P3IN+6
               *.))
06350        IF(AM4Q2.GT.1.) GO TO 702
06370        GO TO 122
06390   702  A44Q=SQRT(AM4Q2)
06410        SA4Q2=(P4P3IN+6.)/(7.*P4P3IN*AM4Q2)
```

```
06450        AMD34=ASIN(SQRT(SAMD2))
06470        DEL34M=AL34.-AMD34
06490        DEL46R=DEL34M
06510        M=0
06530        AL46=0.2/57.3
06535        REG=0
06550        DO 120 JJ=1,90
06570        AL46=AL46+1./57.3
06590   704  AM4SA2=AM4O2*(SIN(AL46))*SIN(AL46)
06610        CDEL46=(((1.2*AM4O2)/(AM4SA2-1))-1)*TAN(AL46)
06630        XCD46=1./CDEL46
06650        DEL46=ATAN(XCD46)
06670        IF(DEL46.LE.0.0) GO TO 120
06690        ALMDEL=AL46-DEL46
06710        AK62=(1./((SIN(ALMDEL))*SIN(ALMDEL)))*(AM4SA2+5.)/(7.*AM4SA2-1)
06730        IF(AK62.LE.1.0) GO TO 120
06750        DCRIT=0.0001
06770        DDEL46=DEL46-DEL46R
06790        IF(ABS(DDEL46).LE.DCRIT) GO TO 130
06810        IF(DDEL46.LT.0.0) GO TO 120
06830        AL46=AL46-0.001/57.3
06850        M=M+1
06870        IF(M.GT.10000) GO TO 122
06890        GO TO 704
06910   120  CONTINUE
06911  C     IF REG REFLECTION NOT POSSIBLE, GO TO MACH STEM SOLUTION
06912  C     OTHERWISE CALCULATE REG. REF. PRESSURE P6
06930        GO TO 122
06970   130  BCR=19
06975        REG=1
07010        SAL462=(SIN(AL46))*SIN(AL46)
07030        P6P4=(7*AM4O2*SAL462-1)/6
07090        P6=P6P4*P4P3(2)*PMP1*P1
07110        PMAXP1=P6/P1
07111  C     REGULAR REFLECTION DURATION(DREG)
07130        AL46=AL46*57.3
```

```
07150       DEL46=DEL46*57.3
07170       R4R3=(6.*AM3O2*SAL34W)/(AM3O2*SAL34W+5.)
07190       R6R4=(6.*AM4SA2)/(AM4SA2+5.)
07210       R6R3=R6R4*R4R3
07230       P6P3=P6P4*P4P3(2)
07250       A62=A3W2*P6P3/R6R3
07270       V6W=-SQRT(AM62)*SQRT(A62)
07290       V6W=V60+ABS(VOWT2)
07310       AMOEFF=SQRT((6.*P6P3+1.)/7.)
07330       VO3EFF=AMOEFF*SQRT(A3W2)
07350       VOWEFF=VO3EFF+V3WWT
07410    91 DREG=(1000000.*X/COS(THETCR))*(1./V6W-1./VOWEFF)
07471 C     SKIP OVER MACH SOLUTION SINCE REG. REF. OCCURRED
07490       GO TO 800
07510 C     MACH STEM PRESSURE(PNS) AND PULSE DURATION(DNS)
07536   122 BSTEM=BETAD
07538       B=1.
07540       IF(AL.NE.O.AND.K.NE.1) B=1.1
07570       P4P3NS=(7.*AM3O2-1.)/6.
07572       P4P3NS=P4P3NS*B
07574       AM3O2=(6.*P4P3NS+1.)/7.
07576       R6R3=6.*AM3O2/(AM3O2+5.)
07577       A62=A3W2*P4P3NS/R6R3
07578       AM6O2=(AM3O2+5.)/(7.*AM3O2-1.)
07579       V6W=-SQRT(AM6O2)*SQRT(A62)
07580       V6W=V60+ABS(VQWT2)
07581       VBW=-SQRT(A62)+V6O+VQWT2
07582       VO3EFF=SQRT(AM3O2)*SQRT(A3W2)
07583       VOWEFF=VO3EFF+V3WWT
07584 C     STEM VELOCITY REL. TO CONE FLOW(VO3EFF AND REL . TO CONE
07585 C     SURFACE(VOWEFF)
07590       U2W=(VB-V2BT)*COS(BETA)+V1*COS(AL)
07595       V2W=(VB-V2BT)*SIN(BETA)+V1*SIN(AL)
07596 C     DEFINE QUASI STEADY CONDITIONS BEHIND MACH STEM
07600       ALE=ATAN(V2W/U2W)
07605       V2WT=(U2W*U2W+V2W*V2W)**.5
```

```
07610       A12=V2WT/SQRT(A22)
07620       BK=COS(ALE)*SIN(TCR)
07625       CK=SIN(ALE)*COS(TCR)
07630       CGAM=BK+CK
07635       PA=P2P1*P1
07640       POS=PA+.5*R2R1*R1*V2WT**2*CGAM*(2-.46/AM2)*CGAM*.46/AM2)/(
07645      *144*32.2)
07650       POSPN=POS/(P5P1*P1)
07655       AMQS=(6*POSPN+1.)/7.
07660       V3QS=SQRT(AMQS)*SQRT(A3N2)
07665       ROSRN=6*AMQS/(AMQS+5.)
07670       V3SO=V3QS*V3NWT
07675       AQS2=A3N2*POSPN/ROSRN
07680       AMQS6=(AMQS+5.)/(7*AMQS-1.)
07685       V3S6=-SQRT(AMQS6)*SQRT(AQS2)
07690       V3S6N=V3S6+V3SO
07691 C     QUASI STEADY PRESSURE(POS),VELOCITY REL. TO CONE(V3S6N)
07695       T=1000000*X/(CJS(TCR)*V3WEFF=)
07700       DNS=(V3WEFF-V3S6N)*T/V3S6N
07710       PMAXNS=P4P3NS*P4P1*P1
07330       PMAXP1=PMAXNS/P1
07332       IF(ALPHA.EQ.0..AND.BETA.EQ.0) GO TO 5
07868 C     PLEEO,DLEEO ARE PRESSURE AND DURATION AT BETA=0 CALCULATED WITH
07869 C     WINDWARD ANALYSIS,USED TO SCALE MORE APPROX LEE PRESSURES
07872       GO TO 900
07873 5     PLEEO=PMAXNS
07874       DLEEO=DNS
07877       IF(K.EQ.1) GO TO 900
07970 800   CONTINUE
08000 C     INITIALIZE FOR LEEWARD ANALYSIS
08020       IF(ALD.EQ.0) GO TO 38
08040       P4P1L=P4P1LE
08060       P4P1L=P4P1LE
08080       V3NL=V3NLEE
08100       GO TO 37
08120 38    CONTINUE
```

```
08140        P6P1L=P.P010
08160        P6P1L=3.G31B
08180        V3.3L=V3.0
08200  C     DEFINE BETA=30S WHERE PRESSURE BEHIND STEM(PSTEM)=QUASI
08202  C     STEADY PRESSURE(POS)
08220        A6P1L=P6P1L*A1**2/3.R81L
08240        IF(KCHECK.EQ.1) GO TO 25
08255        A=1.
08256  C     DEFINE XBETA AND OTHER X SUBSCRIPTED VARIABLES AS DUMMIES
08257  C     FOR THE CALCULATION OF BOS
08260        DO 24  4P=1,90
08280        XBETA=(4P-1)/57.3
08290        XBETAD=XBETA*57.3
08300        XBE=XBETA-ALD/57.3
08320        U=VB*CJS(XBE)+V1
08340        V=V3*SIN(XBE)
08360        VB.IX=(U*U+V*V)**.5
08380        D=ATAN(V/U)
08400        BHD=XBE-D
08420        BMT=XBETA-TCR
08440        VQWX=VB.IX*CJS(BHD)/CJS(BMT)
08460        VQ3X=VQWX-V3WL
08480        A46X2=VQ3X*VQ3X/AW2L
08500        P6P3X=(7*A46X2-1)/6.
08520        PSTEM=P6P3X**P6P1L*P1
08540        IF(XBETA.NE.0) GO TO 7
08541  C     PREF IS LEESIDE PRESSURE(PLEE) AT BETA=0 CALCULATED WITH
08542  C     TRANS. WAVE ASSUMED STRAIGHT,USED TO NON DIM. LEESIDE PRESS.
08560        PREF=PSTEM
08580  7     CONTINUE
08600        PSTEM=PSTEM*PLEEO/PREF
08620        U2WX=(VB-V2BT)*COS(XBETA)+V1*COS(AL)
08640        V2WX=(VB-V2BT)*SIN(XBETA)+V1*SIN(AL)
08660        ALE=ATAN(V2WX/U2WX)
08680        THETB=TCR-AL
08700        V2WTX=(V2WX*V2WX+U2WX*U2WX)**.5
```

56

```
08720      A22=V2MTX/SINT(A22)
08740      CPHI=SIN(TCR)*COS(ALE)-COS(TCR)*SIN(ALE)
08760      PA=P2P1*A
08765      PB=.5*P2R1*R1*V2MTX**2.*CPHI*((2.-.46/AM2)*CPHI+.46/AM2)/(144*32.2
08770     *)
08775      POS=PA+PB
08800      IF(PSTEM.LT.POS) GO TO 23
08802      IF(GP.GT.21) GO TO 23
08840  24 CONTINUE
08841 C  BETA AT WHICH PRESS. BEHIND STEM EQUALS QUASI STEADY PRESS.
08842 C  (BOS) IS DEFINED HERE
08860  23 BOS=XBETA
08880      KCHECK=1
08885      IF(BOS.LT.0.087) BOS=0.087
08900      BOSD=BOS*57.3
08901 C  CALCULATE LEEWARD PRESSURE(PLEE) AND DURATION(DURALE)
08940  25 CONTINUE
08960      U=VD*COS(BE)+V1
08960      V=V3*SIN(BE)
09000      VBMT=(U*U+V*V)**.5
09020      D=ATAN(V/U)
09040      BMD=BE-D
09060      BMT=BETA-TCR
09080      VQWLEE=VBMT*COS(BMD)/COS(BMT)
09100      VQ3LEE=VQWLEE-V3WL
09120      AMQ3L2=VQ3LEE*VQ3LEE/AW2L
09140      P6P3LE=(7.*AMQ3L2-1)/6.
09141 C  CALC. PLEE FIRST WITH STRAIGHT TRANS. WAVE ASSUMPTION
09142 C  THEN CORRECT PLEE WITH RATIO PLEEQ/PREF
09160      PLEE=P6P3LE*PWP1L*P1
09180      PLEE=PLEE*RLEEQ/PREF
09200      P6P3LE=PLEF/(PWP1L*P1)
09220      AMQ3L2=(6*P6P3LE+1.)/7.
09240      R6R3LE=6.*AMQ3L2/(AMQ3L2+5.)
09260      A6LEE2=AW2L*P6P3LE/R6R3LE
09280      AM6QL2=(AMQ3L2+5.)/(7.*AMQ3L2-1.)
```

```
09300        V6QLEE=-SQRT(A6QL2)*SQRT(A6LEE2)
09305        VQ3LEE=SQRT(AMQ3L2)*SQRT(AM2L)
09310        VQMLEE=VQ3LEE*V3ML
09320        V6LEE=V6QLEE+VQMLEE
09340        DLEE=(1000000.*X/COS(TCR))*((VQMLEE-V6MLEE)/(V6LEE*VQMLEE))
09360        IF(BQS.EQ.0) GO TO 202
09380        DURALE=-DLEE*BETA/BQS+DLEE
09400        GO TO 203
09420    202 DURALE=0
09440 C     BETA GREATER THAN BQS
09460    203 U2M=(VB-V2BT)*COS(BETA)+V1*COS(AL)
09462        V2M=(VB-V2BT)*SIN(BETA)+V1*SIN(AL)
09464        ALE=ATAN(V2M/U2M)
09466        V2MT=(U2M*U2M+V2M*V2M)**.5
09468        AM2=V2MT/SQRT(A22)
09480        IF(BETA.LT.BQS) GO TO 36
09500        V2WT=(V2M*V2M+U2M*U2M)**.5
09520        AM2=V2MT/SQRT(A22)
09540        THETE=TCR-AL
09560        CPHI=SIN(TCR)*COS(ALE)-COS(TCR)*SIN(ALE)
09580        PC=.5*R2R1*R1*V2MT**2*CPHI*((2-.46/AM2)*CPHI+.46/AM2)/(144*32.2)
09600        PLEE=PA+PC
09620        P6P3LE=PLEE/(PMP1L*P1)
09640        AMQ3L2=(6.*P6P3LE+1)/7.
09660        VQ3LEE=SQRT(AMQ3L2)*SQRT(AM2L)
09680        VQMLEE=VQ3LEE+V3MI
09700        DURALE=0
09720     36 CONTINUE
09780        ENGTIM=(1Q0000.*X/COS(TCR))*(1./VQMLEE-1./VQMEFF)
09782        IF(BETA.EQ.0) ENGTIM=0
09833        WRITE(6,34)ENGTIM
09840     34 FORMAT(/6X,'ENGULFMENT TIME(MICRO-SEC)=',F8.2)
09842        WRITE(6,39)
09844     39 FORMAT(//6X,'CIRCUMFERENTIAL',10X,'PRE-ENCOUNTER',10X,'PEAK PRESSU
09846       *RE',11X,'QUASI-STEADY',9X,'PULSE DURATION'/7X,'ANGLE,PHI-DEG',12
09848       *X,'PRESSURE-PSI',15X,'PSI',16X,'PRESSURE-PSI',10X,'MICRO-SEC')
```

58

```
09900 C    CIRC...  ...TIAL DISTRIBUTION OF PRESSURE(PC) AND PULSE
09901 C    ...
09902      DO IJ=1,10
09904      PHI=(IJ-1)*20./57.3
09906      PHIJ=PHI*5/.3
09907      PHIA=PHI/2
09890      IF(BETA.EQ.0..AND.ALO.EQ.0) GO TO 9
09900      AK=VOWLEE/VOWEFF
09900      AK1=(1.+AK)/(1.-AK)
09921 C    AK2=(1.-AK1)*VOWEFF
09940 C    ...AVE FRONT VELOCITY REL TO SURFACE
09960      VQ=AK2/(COS(PHI)-AK1)
09 9      IF(BETA.EQ.0..AND.ALO.EQ.0) VQ=VOWEFF
09980      PWP1C=PWP1U
10000      RWR1C=RWR1U
10020      AW2C=A3W2
10040      V3WC=V3WWT
10060      IF(ALPHA.EQ.0) GO TO 10
10080 C    ESTIMATE PRE-ENCOUNTER SURFACE PRESSURE,SND SPD AND VELOCITY
10100      PHIX=PHI/2
10120      PWP1C=PWP1W-(PWP1W-PWP1LE)*(SIN(PHIX))**2
10140      RWR1C=RWR1W-(RWR1W-RWR1LE)*(SIN(PHIX))**2
10160      AW2C=PWP1C*A1**2/RWR1C
10180      V3WC=VW+(V3WLEE-VW)*(SIN(PHIX))**2
10181      PI=PWP1C*P1
10200 10   CONTINUE
10220      V3=VQ-V3WC
10240      AMO=V3*V3/AW2C
10260      P6P3=(7.*AMO-1.)/6
10280      PC=P6P3*PWP1C*P1
10320 C    QUASI STEADY PRESSURE
10344      BK=COS(ALE)*SIN(TCR)
10346      CK=SIN(ALE)*COS(TCR)
10348      CGAM=BK+CK*COS(PHI)
10350      PD=PA
10360      PQS=PD+.5*R2R1*R1*V2WT**2*CGAM*((2.-.46/AM2)*CGAM+.46/AM2)/(
```

59

```
10300        *144=32.2)
10440    C    PULSE DURATION
10442        DH=0.5
10444        DL=DURALE
10446        IF(FREG.EQ.1)DH=FREG
10448        DURA=0.-(DH-DL)*(SIN(PHIX))**2
10450        RGR3=6.*A132/(A10+5.)
10460        A62=1.12C*P623/R6R3
10500        A3602C=(A103+5.)/(7.*AM0-1.)
10520        V60C=-SQRT(A3602C)*SQRT(A62)
10540        V6HC=V60C+VO
10560        DC=(1000000*X/COS(TCR))*((VO-V6HC)/(VO=EFF*V5HC))
10562        PQSP.=POS/(P*PIC*P1)
10564        AM0S=(6.*PQSP*1.)/7.
10565        V30S=SQRT(AM0S)*SQRT(AN2C)
10566        RQSR4=6.*AM0S/(AM0S+5.)
10567        VQS0=V30S+V34C
10568        AQS2=A.12C*PQSP4/RQSR4
10569        A.10S6=(AM0S+5.)/(7.*AMQS-1.)
10570        VQS6=-SQRT(AEQS6)*SQRT(AQS2)
10572        VQS6M=VQS6+VQSO
10573        T=1000000*X/(COS(TCR)*VQMEFF)
10574        DOS=(VQSO-VQS6M)*T/VQS6M
10576        D=(VQ-VQS6M)*T/VQS6M
10578        IF(POS.GE.PC)D=0.
10600        WRITE(6,40)PHID,PI,PC,POS,DURA
10602    40  FORMAT(10X,F7.2,16X,F8.2,15X,F8.2,15X,F8.2,15X,F8.2)
10620    3   CONTINUE
10640    302 CONTINUE
10660    900 CONTINUE
10680    901 CONTINUE
10700        STOP
10720        END
```

5.0 CONCLUSIONS

The primary conclusion drawn from this study was that it is
possible to formulate a reasonably accurate semi-empirical model of the
shock-on-shock phenomenon. As with any such model the range of appli-
cability, until it's demonstrated otherwise, is assumed to be limited to
the range of parameters for which test data are available. However, the
empiricism was kept to a level which should allow the model to be used
effectively over a much larger range of conditions (i.e., blast strengths)
than that covered by the existing data.

The model is cost effective in that a set of encounter angles can
be examined with no more than a few seconds of CPU time on the IBM
370/158.

The model deals effectively with small angles of attack, but must
become increasingly suspect as the angle of attack exceeds the cone
half-angle. This caution is noted because very little test data are
available for a cone at angle of attack in a blast environment to
compare the accuracy of the prediction method, and because of the
occurrence of flow separation on the leeside of the cone when the angle
of attack exceeds the cone half-angle (approximately). The occurrence
of separation is not accounted for in this model and, therefore, is a
possible improvement that should be addressed as a future task.

REFERENCES

1. Kutler, P. and Sakell, L., 1"Three-Dimensional, Shock-on-Shock Interaction Problem," AIAA paper No. 75-49, San Diego, California, January 1975.

2. Reutenik, J. R., et al, Shock-on-Shock Measurements At Mach 3 and 5 From Rocket-Propelled Sled Tests, Phases 2 and 3: Oblique Intercepts, Defense Nuclear Agency Report DNA 3813F-1, Nov. 1975.

3. Aiello, G. F., Support of Phase II and III of the Shock-on-Shock Sled Test Program, Defense Nuclear Agency Report DNA 3787F, October 1975.

4. Inger, G. R., "Oblique Blast Impingement on Slender Hypersonic Bodies," AIAA Journal, Vol. R, No. 8, August 1966, pp 1475-1477.

5. McNamara, W., "FLAME Computer Code for the Axisymmetric Interaction of a Blast Wave with a Shock Layer on a Blunt Body," Journal of Spacecraft and Rockets, Vol 4, No. 6, June 1967, pp 790.

6. Taylor, T. D., "Shock-Shock Interaction Theory Including Real Gas and Three-Dimensional Effects," Aeroneutronic Research Laboratory, Prepared for Picatinny Arsenal, Technical Report No. 3319, April 1966.

7. Brown, E. A. and Mullaney, G. J., "Experiments on the Head-on Shock-Shock Interaction," AIAA Journal, Vol. 3, No. 11, November 1965, pp 2168-2170.

8. Merritt, D. L. and Aronson, R. M., "Wind Tunnel Simulation of Head-on Bow Wave-Blast Wave Interactions," Naval Ordnance Laboratory, NOLTR 67-123, August 1967.

9. Merritt, D. L. and Aronson, P. M., "Experimental Studies of Shock-Shock Interactions on a Nine Degree Cone," NOLTR 67-182, January 1968.

10. Baltakis, F. P., "Shock Interaction Surface Pressures for Hemispherical and Conical Bodies," NOLTR 71-27, February 1971.

11. Ames Research Staff, Equations, Tables, and Charts for Compressible Flow, NACA Report 1135, 1953.

12. Kutler, P., Letter to Martin Marietta from National Aeronautics and Space Administration, Ames Research Center, March 28, 1975.

13. The Martin Marietta Approach to Interceptor Missile Subsystem SPRINT, Vol. I Appendix, Martin Marietta Report OR 2900P, Feb. 1963 (Confidential).

14. Smyrl, J. L., The Impact of a Shock Wave on a Thin Two-Dimensional Airfoil Moving at Supersonic Speeds, Journal of Fluid Mechanics, Vol. 4, 1963.

DISTRIBUTION LIST

DEPARTMENT OF DEFENSE

Director
Defense Advanced Rsch Proj Agency
Architect Building
1400 Wilson Blvd.
Arlington, VA 22209
  ATTN: Strategic Tech Office   1

Defense Documentation Center
Cameron Station
Alexandria, VA 22314
  ATTN: TC   12

Director
Defense Intelligence Agency
Washington, DC 20301
  ATTN: DT-7D   1
  ATTN: DT-1C Nuc Eng Branch   1
  ATTN: DT-2 WPNS & Sys Div   1

Director
Defense Nuclear Agency
Washington, DC 20305
  ATTN: STTL Tech Library   3
  ATTN: STST Archives   1
  ATTN: DDST   1
  ATTN: SPAS   3
  ATTN: STSP   1

Dir of Defense RSCH & Engineering
Department of Defense
Washington, DC 20301
  ATTN: DD/S&SS   1
  ATTN: AD/OS   1
  ATTNL AD/DS   1

Commander
Field Command
Defense Nuclear Agency
Kirtland AFB, NM 87115
  ATTN: FCTMOF   1
  ATNN: FCPR   1
  ATTN: FCTMD   1

NAME	COPIES

Director
Joint Strat Tgt Planning Staff JCS
Offutt AFB
Omaha, NB 68113
  ATTN: JLTW-2   1
  ATTN: JPTM   1
  ATTN: JPTP   1

Chief
Livermore Division Fld Command DNA
Lawrence Livermore Laboratory
P.O. Box 808
Livermore, CA 94550
  ATTN: FCPRL   1

DEPARTMENT OF ARMY

Program Manager
BMD Program Office
1300 Wilson Blvd.
Arlington, VA 22209
  ATTN: DACS-BMZ   1
  ATTN: DACS-BMT John Shea   1
  ATTN: DACS-BMZ-D Julian Davidson   1
  ATTN: DACS-BMT Clifford E. McLain   1

Command
BMD System Command
P.O. Box 1500
Huntsville, AL 35807
  ATTN: BDMSC-TEN Noah J. Hurst   1

Dep Chief of Staff for RSCH Dev & Acq
Department of the Army
Washington, DC 20310
  ATTN: NCB Division   1

Deputy Chief of Staff for OPS & Plans
Department of the Army
Washington, DC 20310
  ATTN: Dir of Chem & Nuc Ops   1

Commander
Harry Diamond Laboratories
2800 Powder Mill Road
Adelphi, MD 20783
  ATTN: DRXDO-RC Robert B. Oswald, Jr.   1
  ATTN: DRXDO-NP   1
  ATTN: DRXDO-RBH James H. Gwaltney   1

NAME	COPIES
Commander	
Picatinny Arsenal	
Dover, NJ 07801	
ATTN: SMUPA-MD Henry Opat	1
ATTN: SARPA-ND-C-T Donald Miller	1
ATTN: SARPA-FR-E Louis Avrami	1
Commander	
Trasana	
White Sands Missile Range, NM 88002	
ATTN: R.E.Dekinder, Jr.	1
Director	
U.S. Army Ballistic Research Labs	
Aberdeen Proving Ground, MD 21005	
ATTN: Robert E. Eichelberger	1
ATTN: DRXBR-TB J.T. Frasier	1
ATTN: DRXRD-BVL William J. Schuman, Jr.	1
Commander	
U.S. Army Mat & Mechanics Rsch Ctr	
Watertown, MA 02172	
ATTN: DRXMR-HH John F. Dignam	1
Command	
U.S. Army Materiel Dev & Readiness Cmd	
5001 Eisenhower Avenue	
Alexandria, VA 22333	
ATTN: DRCDE-D Lawrence Flynn	1
Commander	
U.S. Army Missile Command	
Redstone Arsenal, AL 35809	
ATTN: DRSMI-XS Chief Scientist	1
ATTN: DRSMI-RRR Bud Gibson	1
ATTN: DRS-RKP W.B. Thomas	1
ATTN: DRCPM-PE-EA Wallace O. Wagner	1
Commander	
U.S. Army Nuclear Agency	
Fort Bliss, TX 79916	
ATTN: ATCA-NAW	1

DEPARTMENT OF NAVY

Chief of Naval Material	
Navy Department	
Washington, DC 20360	
ATTN: Mat 0323 Irving Jaffe	1

Chief of Naval Research
Navy Department
Arlington, VA 22217
  ATTN: Code 464 Thomas P. Quinn   1

Director
Naval Research Laboratory
Washington, DC 20375
  ATTN: Gerald Copperstein Code 7770   1
  ATTN: Code 5180 Mario A. Persechino   1
  ATTN: Code 2027 Tech Lib   1

Commander
Naval Sea Systems Command
Navy Department
Washington, DC 20362
  ATTN: 0333A Marlin A. Kinna   1

Commander
Naval Surface Weapons Center
White Oak, Silver Spring, MD 20910
  ATTN: Code 323 W. Carson Lyons   1
  ATTN: Code WA501 Navy Nuc Prgms Off 1
  ATTN: Code 2302 Leo F. Gowen   1

Director
Strategic Systems Project Office
Navy Department
Washington, DC 20376
  ATTN: NSP-272 CDR Leslie Stoessl   1

DEPARTMENT OF THE AIR FORCE

AF Materials Laboratory, AFSC
Wright-Patterson AFB, OH 45433
  ATTN: MAS   1
  ATTN: MBC Donald L. Schmidt   1
  ATTN: T. Nicholas   1

AF Rocket Propulsion Laboratory, AFSC
Edwards AFB, CA 93523
  ATTN: RTSN G.A. Beale   1

AF Weapons Laboratory, AFSC
Kirtland AFB, NM 87117
  ATTN: SUL   1
  ATTN: DYS Lt. F.J. Burns   1
  ATTN: DYV   1
  ATTN: Dr. Minge   1

NAME	COPIES

Commander
Foreign Technology Division, AFSC
Wright-Patterson AFB, OH 45433
  ATTN: TDFRD J. D. Pumphrey   1
  ATTN: TDPTN   1

Hq USAF/RD
Washington, DC 20330
  ATTN: RD   1

SAMSO/MN
Norton AFB, CA 92409
(Minuteman)
  ATTN: MNNR   1

SAMSO/RS
Post Office Box 92960
Worldway Postal Center
Los Angeles, CA 90009
(Reentry Systems)
  ATTN: RSSF   1
  ATTN: RSS   1

Command in Chief
Strategic Air Command
Offutt AFB, NB 68113
  ATTN: DOXT   1
  ATTN: XPFS   1

U.S. ENERGY RESEARCH AND DEVELOPMENT ADMINISTRATION

Division of Military Application
U.S. Energy Rsch & Dev Admin
Washington, DC 20545
  ATTN: Doc Con for Res & Dev Branch   1
  ATTN: Doc Con for CDR Richard E. Peterson   1
  ATTN: Doc Con for LTC Donald L. McNutt   1

University of California
Lawrence Livermore Laboratory
P.O. Box 808
Livermore CA 94550
  ATTN: C. Joseph Taylor L-92   1
  ATTN: Joseph E. Keller, Jr. L-125   1
  ATTN: G. Staihle L-24   1

Los Alamos Scientific Laboratory
P.O. Box 1663
Los Alamos, NM 87545
  ATTN: Doc Con for J.W. Taylor   1
  ATTN: Doc Control for John McQueen   1
  ATTN: Doc Control for R.S. Thurston   1

Sandia Laboratories
Livermore Laboratory
P.O. Box 969
Livermore, CA 94550
  ATTN: Raymond NG   1
  ATTN: Doc Control for T. Gold   1
  ATTN: Doc Control for C.S. Hoyle   1
  ATTN: Doc Con for 8131 H.F. Norris, Jr.   1

Sandia Laboratories
P.O. Box 5800
Albuquerque, NM 87115
  ATTN: Doc Con for Albert Chabai   1
  ATTN: Doc Con for R.R. Boade   1
  ATTN: Doc Control for D. McCloskey   1

DEPARTMENT OF DEFENSE CONTRACTORS

Aeronautical Rsch Assoc of Princeton Inc.
50 Washington Road
Princeton, NJ 08540
  ATTN: Coleman Donaldson   1

Aeronutronic Ford Corporation
Aerospace & Communications Ops
Aeronutronic Division
Ford & Jamboree Roads
Newport Beach, CA 92663
  ATTN: P. Spangler   1

Aerospace Corporation
P.O. Box 92957
Los Angeles, CA 90009
  ATTN: W. Barry   1
  ATTN: R. Allen   1
  ATTN: Richard Crolius A2-RM1027   1

AVCO Research & Systems Group
201 Lowell Street
Wilmington, MA 01887
  ATTN: John Gilmore E502   1
  ATTN: John E. Stevens E500   1

NAME	COPIES

Battelle Memorial Institute
505 King Avenue
Columbus, OH 43201
  ATTN: Merwyn R. Vanderlind   1
  ATTN: W. Pfeifer   1

Boeing Company, The
P.O. Box 3707
Seattle, WA 98124
  ATTN: Brian Lempriere   1

Brown Engineering Company, Inc.
Cummings Research Park
Huntsville, AL 35807
  ATTN: Ronald Patrick   1

Effects Technology, Inc.
5383 Hollister Avenue
Santa Barbara, CA 93111
  ATTN: Robert Wengler   1

General Electric Company
Space Division
Valley Forge Space Center
Goddard Blvd King of Prussia
P.O. Box 8555
Philadelphia, PA 19101
  ATTN: G. Harrison   1
  ATTN: Carl Anderson   1
  ATTN: Philip Cline Rm 3700   1

General Electric Company
Tempo-Center for Advanced Studies
816 State Street (P.O. Drawer QQ)
Santa Barbara, CA 93102
  ATTN: DASTAC   1

Institute for Defense Analysis
400 Army-Navy Drive
Arlington, VA 22202
  ATTN: Joel Bengston   1
  ATTN: Ida Librarian Ruth S. Smith   1

Kaman Avidyne
Division of Kaman Sciences Corp
83 Second Avenue
Northwest Industrial Park
Burlington, MA 01803
  ATTN: Norman P. Hobbs   1

NAME	COPIES

Kaman Sciences Corporation
P.O. Box 7463
Colorado Springs, CO 80933
  ATTN: Albert P. Bridges   1
  ATTN: Thomas Meagher   1
  ATTN: Frank H. Shelton   1
  ATTN: Jerry L. Harper   1
  ATTN: John R. Hoffman   1

Lockheed Missiles and Space Company
3251 Hanover Street
Palo Alto, CA 94304
  ATTN: A.P. Hardt   1
  ATTN: Lloyd F. Chase   1
  ATTN: Raymond R. Capiaux   1
  ATTN: F.G. Borgardt   1

Martin Marietta Aerospace
Orlando Division
P.O. Box 5837
Orlando, FL 32805
  ATTN: Laird Kinnaird   1

McDonnell Douglas Corporation
5301 Bolsa Avenue
Huntington Beach, CA 92647
  ATTN: L. Cohen   1
  ATTN: J. Kirby   1
  ATTN: J.F. Garibotti   1
  ATTN: R.J. Reck   1

Physics International Company
2700 Merced Street
San Leandro, CA 94577
  ATTN: Doc Con for James Shea   1

Prototype Development Associates Inc.
1740 Garry Avenue
Santa Ana, CA 92705
  ATTN: John Slaughter   1

R&D Associates
P.O. Box 9695
Marina Del Rey, CA 90291
  ATTN: Albert L. Latter   1
  ATTN: Jerry Carpenter   1
  ATTN: Harold L. Brode   1
  ATTN: F.A. Field   1

NAME	COPIES

Science Applications, Inc.
P.O. Box 2351
La Jolla, CA 92038
  ATTN: R. Fisher
  ATTN: G. Ray
	
	1
	1

Science Applications, Inc. 101 Continental Blvd. Fl Segundo, CA 90245 ATTN: J. Courtney	 1
Southern Research Institute 2000 Ninth Avenue South Birmingham, AL 35205 ATTN: C.D. Pears	 1

Stanford Research Institute
333 Ravenswood Avenue
Monlo Park, CA 94025
  ATTN: Donald Curran
  ATTN: Herbert E. Lindberg
  ATTN: George R. Abrahamson
	
	1
	1
	1

Stanford Research Institute 306 Wynn Drive, N.W. Huntsville, AL 35805 ATTN: Harold Carey	 1